Ann. Geophys., 24, 2553–2572, 2006
www.ann-geophys.net/24/2553/2006/

Annales Geophysicae

The role of the zonal $E \times B$ plasma drift in the low-latitude ionosphere at high solar activity near equinox from a new three-dimensional theoretical model

A. V. Pavlov

Pushkov Institute of Terrestrial Magnetism, Ionosphere and Radio-Wave Propagation, Russian Academy of Science (IZMIRAN), Troitsk, Moscow Region, 142190, Russia

Received: 2 May 2006 – Revised: 22 August 2006 – Accepted: 31 August 2006 – Published: 20 October 2006

Abstract. A new three-dimensional, time-dependent theoretical model of the Earth's low and middle latitude ionosphere and plasmasphere has been developed, to take into account the effects of the zonal $\boldsymbol{E}\times\boldsymbol{B}$ plasma drift on the electron and ion number densities and temperatures, where $\boldsymbol{E}$ and $\boldsymbol{B}$ are the electric and geomagnetic fields, respectively. The model calculates the number densities of $O^+(^4S)$, H^+, NO^+, O_2^+, N_2^+, $O^+(^2D)$, $O^+(^2P)$, $O^+(^4P)$, and $O^+(^2P^*)$ ions, the electron density, the electron and ion temperatures using a combination of the Eulerian and Lagrangian approaches and an eccentric tilted dipole approximation for the geomagnetic field. The F2-layer peak density, *NmF2*, and peak altitude, *hm*F2, which were observed by 16 ionospheric sounders during the 12–13 April 1958 geomagnetically quiet time high solar activity period are compared with those from the model simulation. The reasonable agreement between the measured and modeled *Nm*F2 and *hm*F2 requires the modified equatorial meridional $\boldsymbol{E}\times\boldsymbol{B}$ plasma drift given by the Scherliess and Fejer (1999) model and the modified NRLMSISE-00 atomic oxygen density. In agreement with the generally accepted assumption, the changes in *Nm*F2 due to the zonal $\boldsymbol{E}\times\boldsymbol{B}$ plasma drift are found to be inessential by day, and the influence of the zonal $\boldsymbol{E}\times\boldsymbol{B}$ plasma drift on *Nm*F2 and *hm*F2 is found to be negligible above about 25° and below about –26° geomagnetic latitude, by day and by night. Contrary to common belief, it is shown, for the first time, that the model, which does not take into account the zonal $\boldsymbol{E}\times\boldsymbol{B}$ plasma drift, underestimates night-time *Nm*F2 up to the maximum factor of 2.3 at low geomagnetic latitudes, and this plasma transport in geomagnetic longitude is found to be important in the calculations of *Nm*F2 and *hm*F2 by night from about –20° to about 20° geomagnetic latitude. The longitude dependence of the night-time low-latitude influence of the zonal $\boldsymbol{E}\times\boldsymbol{B}$ plasma drift on *Nm*F2, which is found for the first time, is explained in terms of the longitudinal asymmetry in $\boldsymbol{B}$ (the eccentric magnetic dipole is displaced from the Earth's center and the Earth's eccentric tilted magnetic dipole moment is inclined with respect to the Earth's rotational axis) and the variations of the wind induced plasma drift and the meridional $\boldsymbol{E}\times\boldsymbol{B}$ plasma drift in geomagnetic longitude. The study of the influence of the zonal $\boldsymbol{E}\times\boldsymbol{B}$ plasma drift on the topside low-latitude electron density is presented for the first time.

Keywords. Ionosphere (Electric fields and currents; Equatorial ionosphere; Modeling and forecasting; Plasma temperature and density)

1 Introduction

The ionosphere at the geomagnetic equator and low geomagnetic latitudes have been studied observationally and theoretically for many years (see Moffett, 1979; Anderson, 1981; Walker, 1981; Anderson et al., 1996; Bailey and Balan, 1996; Millward et al., 1996; Roble, 1996; Richards and Torr, 1996; Schunk and Sojka, 1996; Rishbeth, 2000; Abdu, 1997, 2001; Huba et al., 2000; Fesen et al., 2002; Maruyama et al., 2003; Pavlov et al., 2006, and references therein). The behaviour of the equatorial and low-latitude ionosphere is strongly dependent upon the meridional component (which is located in a plane of a geomagnetic meridian) of a drift velocity, $\boldsymbol{V}^E=\boldsymbol{E}\times\boldsymbol{B}/B^2$, of electrons and ions perpendicular to the geomagnetic field, $\boldsymbol{B}$, due to an electric field, $\boldsymbol{E}$, which is generated in the E region. Sterling et al. (1969) found that the effect of the zonal component of $\boldsymbol{V}^E$ (geomagnetic east – geomagnetic west component) on the F2-layer peak density in the low-latitude ionosphere is not significant at solar minimum and solar maximum equinoctial conditions. However, as was pointed out by Anderson (1981), the zonal plasma drift used by Sterling et al. (1969) bears little resemblance to the observed zonal plasma drifts given by Fejer et al. (1981).

Correspondence to: A. V. Pavlov
(pavlov@izmiran.rssi.ru)

Published by Copernicus GmbH on behalf of the European Geosciences Union.

This discrepancy between the measured and plasma drifts used can lead to an incorrect conclusion about the role of the zonal component of the $\boldsymbol{E}\times\boldsymbol{B}$ plasma drift in the low-latitude ionosphere. The average $\boldsymbol{E}\times\boldsymbol{B}$ zonal F-region plasma drift (Fejer et al., 1981) measured over Jicamarca was used by Anderson (1981) to reinvestigate the effects of the zonal $\boldsymbol{E}\times\boldsymbol{B}$ plasma drift on the equatorial F-region ionosphere for high solar activity conditions. Anderson (1981) has found that the F2-layer peak electron densities calculated over the geomagnetic equator at 20:00 LT and at 24:00 LT do not differ significantly from those obtained when the zonal $\boldsymbol{E}\times\boldsymbol{B}$ drift is omitted, while there are noticeable changes in the F2-layer peak altitudes (see Fig. 10 of Anderson, 1981). As a result of the model calculations given by Anderson (1981), effects of the zonal $\boldsymbol{E}\times\boldsymbol{B}$ plasma drift on the electron and ion densities and temperatures were not taken into account in the previous model studies (e.g. Anderson et al., 1996; Bailey and Balan, 1996; Millward et al., 1996; Pavlov, 2003; Pavlov et al., 2004a, b, 2006). The present work revises the relationship between the zonal component of the plasma drift and the dynamics of the low-latitude F2-layer using a new three-dimensional time-dependent model of the low and middle latitude ionosphere and plasmasphere presented in Sect. 2. To test the reliability of the new model, the theoretical study is carried out in the present case study, in which the F2-layer peak electron density, *Nm*F2, and altitude, *hm*F2, are observed simultaneously in the low-latitude ionosphere by the La Paz, Trivandrum, Ahmedabad, Kodaikonal, Tiruchirapalli, Singapore, Maui, Panama, Talara, Chiclayo, Huancayo, and Bogota ionospheric sounders during the 12–13 April 1958 geomagnetically quiet time period at high solar activity.

2 New three-dimensional, time-dependent theoretical model

The two-dimensional, time-dependent model of the low and middle latitude ionosphere and plasmasphere developed by Pavlov (2003) calculates the number densities, N_i, of $O^+(^4S)$, H^+, NO^+, O_2^+, N_2^+, $O^+(^2D)$, $O^+(^2P)$, $O^+(^4P)$, and $O^+(^2P^*)$ ions, N_e, the electron, T_e, and ion, T_i, temperatures in a plane of a geomagnetic meridian in a centered dipole approximation for the geomagnetic field without taking into consideration the zonal plasma drift effects on N_i, N_e, T_e, and T_i. A new three-dimensional time-dependent mathematical model of the low and middle latitude ionosphere and plasmasphere presented in this work includes the two-dimensional time-dependent model given by Pavlov (2003) as a principal block, takes into account the effects of the zonal plasma drift on N_i, N_e, T_e, and T_i , and uses an eccentric tilted dipole approximation for the geomagnetic field to calculate the time-dependent electron and ion densities, and temperatures as a function of latitude, longitude, and altitude on a fixed spatial grid at low and middle latitudes. In the model, the Earth's eccentric tilted magnetic dipole moment is inclined with respect to the Earth's rotational axis but is located at a point which is not coincident with the Earth's center (the first eight nonzero coefficients in the expansion of the geomagnetic field potential in terms of spherical harmonics are taken into account). The dependences of the parameters of the eccentric tilted magnetic dipole on a year are given by Frazer-Smith (1987) and Deminov and Fishchuk (2000). The model includes the production and loss rates of ions by the photochemical reactions described in detail by Pavlov (2003) and Pavlov and Pavlova (2005).

Eccentric dipole orthogonal curvilinear coordinates q, U, and Λ are employed in the model calculations, where q is aligned with, and U and Λ are perpendicular to, the magnetic field, and the U and Λ coordinates are constant along an eccentric dipole magnetic field line. It should be noted that $q=(R_E/R)^2\cos\Theta$, $U=(R_E/R)\sin^2\Theta$, and Λ is the geomagnetic longitude, where R is the radial distance from the geomagnetic field center, $\Theta=90^\circ-\varphi$ is the geomagnetic colatitude, φ is the geomagnetic latitude, R_E is the Earth's radius. In the model, $\boldsymbol{V}^E=V_\Lambda^E\,\boldsymbol{e}_\Lambda+V_U^E\,\boldsymbol{e}_U$, where $V_\Lambda^E=E_U/B$ is the zonal component of $\boldsymbol{V}^E$, $V_U^E=-E_\Lambda/B$ is the meridional component of $\boldsymbol{V}^E$, $\boldsymbol{E}=E_\Lambda\,\boldsymbol{e}_\Lambda+E_U\,\boldsymbol{e}_U$, E_Λ is the Λ (zonal) component of $\boldsymbol{E}$ in the dipole coordinate system, E_U is the U (meridional) component of $\boldsymbol{E}$ in the dipole coordinate system, $\boldsymbol{e}_\Lambda$ and $\boldsymbol{e}_U$ are unit vectors in Λ and U directions, respectively, $\boldsymbol{e}_U$ is directed downward at the geomagnetic equator.

Equations which determine the trajectory of the ionospheric plasma perpendicular to magnetic field lines and the moving coordinate system are derived by Pavlov (2003) as

$$\frac{\partial}{\partial t}U = -E_\Lambda^{\mathrm{eff}} R_E^{-1} B_0^{-1}, \tag{1}$$

$$\frac{\partial}{\partial t}\Lambda = E_U^{\mathrm{eff}} R_E^{-1} B_0^{-1}, \tag{2}$$

where $E_\Lambda^{\mathrm{eff}}=E_\Lambda h_\Lambda R_E^{-1}$, $E_U^{\mathrm{eff}}=E_U\ h_U\ R_E^{-1}$, $h_\Lambda=R\sin\Theta$, $h_U=RU^{-1}\cos I$, R_E is the Earth's radius, I is the magnetic field dip angle, $\cos I=\sin\Theta\,(1+3\cos^2\Theta)^{-1/2}$, B_0 is the value of B for $R=R_E$ and $\Theta=0$.

As a result of the condition of the frozen-in magnetic field lines into the ionospheric and plasmaspheric plasma, the values of the effective zonal and meridional electric fields E_Λ^{eff} and E_U^{eff} are not changed along magnetic field lines (Pavlov, 2003):

$$\frac{\partial}{\partial q}E_\Lambda^{\mathrm{eff}} = 0,\ \frac{\partial}{\partial q}E_U^{\mathrm{eff}} = 0. \tag{3}$$

It is worth noting that the effective zonal and meridional plasma drift velocities $V_\Lambda^{\mathrm{eff}}=E_U^{\mathrm{eff}}\,B_0^{-1}$ and $V_U^{\mathrm{eff}}=-E_\Lambda^{\mathrm{eff}}\,B_0^{-1}$ can be used in Eqs. (1–3) instead of E_U^{eff} and E_Λ^{eff}, respectively, where $V_\Lambda^{\mathrm{eff}}=V_\Lambda^E\,R_E h_\Lambda^{-1}$ and $V_U^{\mathrm{eff}}=V_U^E\,R_E\,h_U^{-1}$.

The model calculates the values of N_i, N_e, T_i, and T_e in the fixed nodes of the fixed Eulerian volume grid at the fixed

universal times UT≡t=t0, t0+Δt, t0+2Δt, and so on, up to the final universal time with the time step Δt. This Eulerian computational grid consists of a distribution of the dipole magnetic field lines in the ionosphere and plasmasphere. One hundred dipole magnetic field lines are used in the model for each fixed value of Λ. The number of the fixed nodes taken along each magnetic field line is 191. Seventy-two model Eulerian (q,U) computational grid planes are located at Λ=0°, 5°,...355°. For each fixed value of Λ, the region of study is a (q,U) plane, which is bounded by two dipole magnetic field lines. The computational grid dipole magnetic field lines are distributed between the low and upper boundary lines. Computational grid dipole magnetic field lines intersect the geomagnetic equatorial point (q=0) at the geomagnetic equatorial crossing heights h^1_{eq}, h^2_{eq}, ... h^{mm}_{eq} with the interval $\Delta h^m_{eq}=h^m_{eq}-h^{m-1}_{eq}$ between neighboring computational grid lines m and m-1, where m=2,... mm, mm=100. The low boundary magnetic field line intersects the geomagnetic equatorial point at the geomagnetic equatorial crossing height h^1_{eq}=150 km. The upper boundary magnetic field line has h^{mm}_{eq}=4264 km.. The computational grid lines have the interval Δh^m_{eq} of 20 km for m=1 and m=2, and the value of Δh^m_{eq} is increased from 20 km to 42 km linearly, if the value of m is changed from m=3 to m=mm.

At each time point, we use the implementation of the Eulerian-Lagrangian method developed by Pavlov (2003) in solving the time dependent and two-dimensional continuity and energy equations at a (q,U) plane and upgrade this method, taking into consideration the plasma drift between the (q,U) planes in geomagnetic longitude. The Eulerian-Lagrangian scheme used describes the plasma evolution based on a reference frame (see Eqs. 1–2) moving with an individual parcel of plasma like a fully Lagrangian method, but makes use an Eulerian computational grid. It involves a forward time integration of Eqs. (1–2). Figure 1 shows schematic illustration of the major elements of the difference between the two-dimensional approach and the three-dimensional approach in the calculations of N_i, T_e, and T_e described below.

Let us assume that the values of N_i(q,U,Λ,t), T_i(q,U,Λ,t), and T_e(q,U,Λ,t) are known, and we calculate the values of N_i(q,U,Λ,t+Δt), T_i(q,U,Λ,t+Δt), and T_e(q,U,Λ, t+Δt) simultaneously for all the computational grid dipole magnetic field lines. The model calculations are carried out in the two parts at each time step. In the first part, the new model uses the algorithms developed by Pavlov (2003) to describe plasma evolution in each (q,U) plane. However, as distinct from the two-dimensional approach of Pavlov (2003), the three-dimensional model results at t+Δt correspond to a (q,U) plane which is located at $\Lambda+\Delta\Lambda$, and this change in geomagnetic longitude (the value of $\Delta\Lambda$) is caused by the zonal $\boldsymbol{E}\times\boldsymbol{B}$ plasma drift. As a result of the first part, the model calculates the values of N_i(q,U,$\Lambda_k+\Delta\Lambda_k$,t+$\Delta$t), T_i(q,U,$\Lambda_k+\Delta\Lambda_k$,t+$\Delta$t), and T_e(q,U,$\Lambda_k+\Delta\Lambda_k$,t+$\Delta$t) from the values of N_i(q,U,Λ_k,t), T_i(q,U,Λ_k,t), and T_e(q,U,Λ_k,t), where k=1,2,... kk. The magnitude of $\Delta\Lambda_k$ is determined from Eq. (2). In the second part, we calculate the values of N_i(q,U,Λ_k,t+Δt), T_i(q,U,Λ_k,t+Δt), and T_e(q,U,Λ_k,t+Δt). In the low-latitude ionosphere, the value of V^E_Λ is positive (an eastward drift of plasma) during the most of the daytime conditions, while during the most of the night-time conditions, the plasma moves westward perpendicular to the geomagnetic field lines in longitude (Fejer et al., 2005; Fejer, 1993). The subsequent strategy of the second part for the case when $V^E_\Lambda>0$ is different from that for the case when $V^E_\Lambda<0$.

At first, we describe the technique in the case when the zonal plasma drift is directed eastward (V^E_Λ(q,U,Λ_k,t)>0). Using the values of N_i(q,U,$\Lambda_k+\Delta\Lambda_k$,t+$\Delta$t), T_i(q,U,$\Lambda_k+\Delta\Lambda_k$,t+$\Delta$t), T_e(q,U,$\Lambda_k+\Delta\Lambda_k$,t+$\Delta$t) and N_i(q,U,$\Lambda_{k-1}+\Delta\Lambda_{k-1}$,t+$\Delta$t), T_i(q,U,$\Lambda_{k-1}+\Delta\Lambda_{k-1}$,t+$\Delta$t), T_e(q,U,$\Lambda_{k-1}+\Delta\Lambda_{k-1}$,t+$\Delta$t), and the interpolation procedure, the model calculates the desired quantities of N_i(q,U,Λ_k,t+Δt), T_i(q,U,Λ_k,t+Δt), and T_e(q,U,Λ_k,t+Δt). It should be noted that the quantities of N_i(q,U,Λ_1,t+Δt), T_i(q,U,Λ_1,t+Δt), and T_e(q,U,Λ_1,t+Δt) are found from the values of N_i(q,U,$\Lambda_1+\Delta\Lambda_1$,t+$\Delta$t), T_i(q,U,$\Lambda_1+\Delta\Lambda_1$,t+$\Delta$t), T_e(q,U,$\Lambda_1+\Delta\Lambda_1$,t+$\Delta$t) and N_i(q,U,$\Lambda_{kk}+\Delta\Lambda_{kk}$,t+$\Delta$t), T_i(q,U,$\Lambda_{kk}+\Delta\Lambda_{kk}$,t+$\Delta$t), T_e(q,U,$\Lambda_{kk}+\Delta\Lambda_{kk}$,t+$\Delta$t), and the interpolation procedure.

If the plasma moves westward, i.e. V^E_Λ(q,U,Λ_k,t)<0, then the technique is changed in comparison with the previous case. The values of N_i(q,U,$\Lambda_k+\Delta\Lambda_k$,t+$\Delta$t), T_i(q,U,$\Lambda_k+\Delta\Lambda_k$,t+$\Delta$t), T_e(q,U,$\Lambda_k+\Delta\Lambda_k$,t+$\Delta$t) and N_i(q,U,$\Lambda_{k-1}+\Delta\Lambda_{k+1}$,t+$\Delta$t), T_i(q,U,$\Lambda_{k+1}+\Delta\Lambda_{k+1}$,t+$\Delta$t), T_e(q,U,$\Lambda_{k+1}+\Delta\Lambda_{k+1}$,t+$\Delta$t), and the interpolation procedure are used to calculate the desired quantities of N_i(q,U,Λ_k,t+Δt), T_i(q,U,Λ_k,t+Δt), and T_e(q,U,Λ_k,t+Δt). Using the interpolation procedure, the values of N_i(q,U,Λ_{kk},t+Δt), T_i(q,U,Λ_{kk},t+Δt), and T_e(q,U,Λ_{kk},t+Δt) are determined from the values of N_i(q,U,$\Lambda_{kk}+\Delta\Lambda_{kk}$,t+$\Delta$t), T_i(q,U,$\Lambda_{kk}+\Delta\Lambda_{kk}$,t+$\Delta$t), T_e(q,U,$\Lambda_{kk}+\Delta\Lambda_{kk}$,t+$\Delta$t) and N_i(q,U,$\Lambda_1+\Delta\Lambda_1$,t+$\Delta$t), T_i(q,U,$\Lambda_1+\Delta\Lambda_1$,t+$\Delta$t), T_e(q,U,$\Lambda_1+\Delta\Lambda_1$,t+$\Delta$t).

If V^E_Λ(q,U,Λ_k,t)=0, then the desired values of N_i(q,U,Λ_k,t+Δt), T_i(q,U,Λ_k,t+Δt), and T_e(q,U,Λ_k,t+Δt) are calculated from N_i(q,U,Λ_k,t), T_i(q,U,Λ_k,t), and T_e(q,U,Λ_k,t), without taking into account the plasma drift between the (q,U) planes in geomagnetic longitude.

As a result, the two-dimensional Eulerian-Lagrangian scheme of Pavlov (2003) was extended to the three-dimensional scheme. The new model works as a time dependent three-dimensional (q, U, and Λ coordinates) global model of the low and middle latitude ionosphere and plasmasphere.

Equations (1–2) determine the trajectory of the ionospheric plasma perpendicular to the magnetic field lines and the moving coordinate system. Time variations of U are determined by time variations of $E^{\rm eff}_\Lambda$, and time variations of Λ

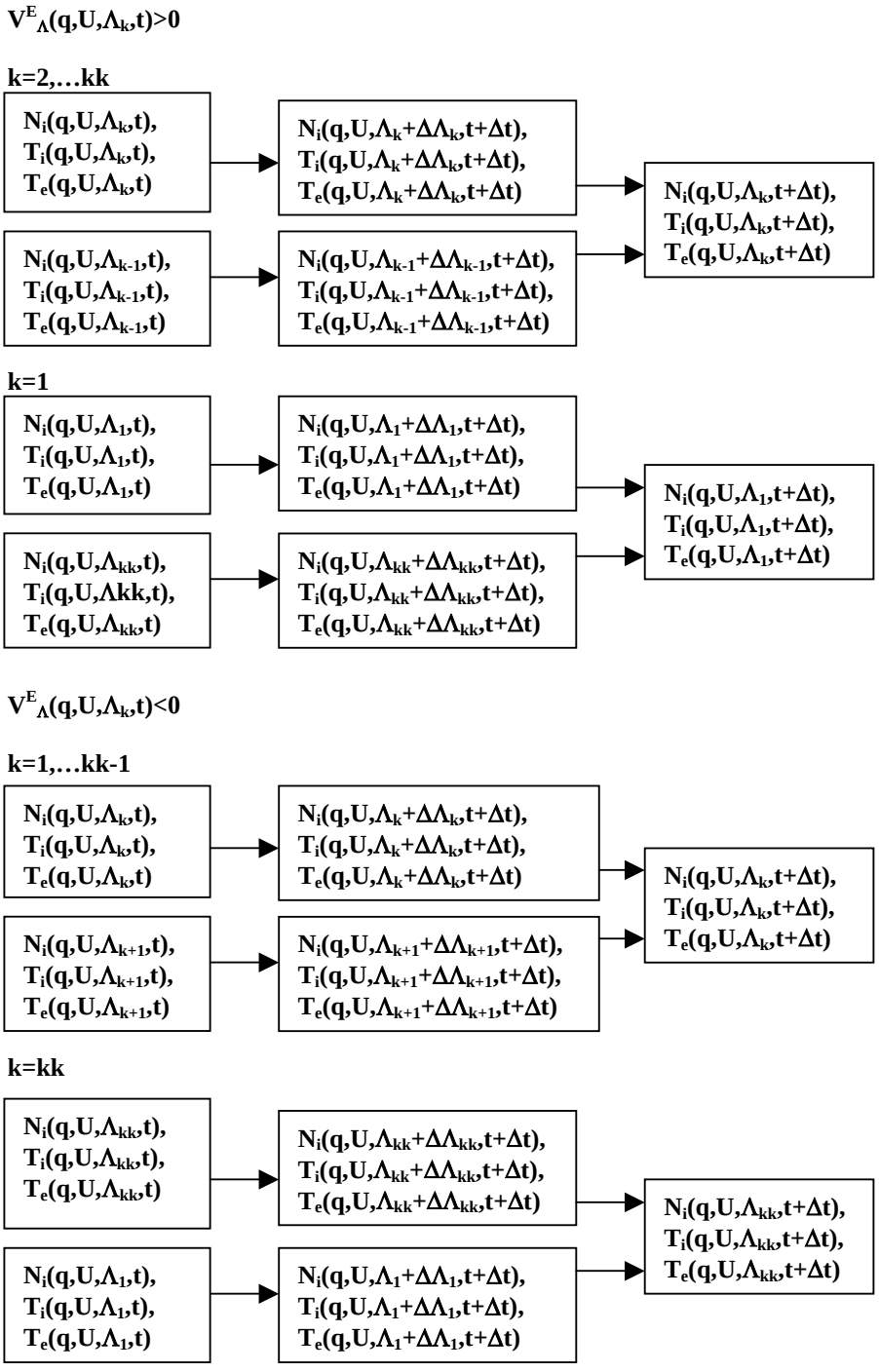

Fig. 1. The major elements of the difference between the two-dimensional approach (Pavlov, 2004) and the three-dimensional approach used in this work in calculations of N_i, T_e, and T_i.

are determined by time variations of $E_U^{\rm eff}$. In the model calculations, the empirical F-region quiet time equatorial vertical drift model of Scherliess and Fejer (1999) is used to calculate the value of E_Λ over the geomagnetic equator at F-region altitudes. The time variations of E_U used in the model simulations over the geomagnetic equator at F-region altitudes are obtained from the time variations of the empirical F-region quiet time equatorial zonal plasma drift shown by the solid line in Fig. 2. The value of this drift velocity is taken from Fig. 2 of Fejer et al. (2005) over Jicamarca for

equinox conditions and F10.7=180. It is assumed that this value of E_U is the same at all geomagnetic longitudes over the geomagnetic equator at F-region altitudes. The equatorial electric fields E_Λ and E_U are used to find the equatorial effective electric fields $E_\Lambda^{\rm eff}$ and $E_U^{\rm eff}$.

The dashed line in Fig. 2 shows the average quiet time zonal plasma drift velocity over Arecibo for equinox conditions at solar maximum taken from Fig. 3 of Fejer (1993). This drift is used to determine the value of E_U at the F-region altitudes over Arecibo. The average quiet time electric field E_Λ at the F-region altitudes over Arecibo is found from the average quiet time perpendicular/northward F-region plasma drift for equinox conditions at solar maximum presented in Fig. 2 of Fejer (1993). The Arecibo values of E_Λ and E_U are used to find the Arecibo quantities of $E_\Lambda^{\rm eff}$ and $E_U^{\rm eff}$. Let a geomagnetic field line intersect the 300-km altitude over the Arecibo radar at a geomagnetic latitude of φ_A. The values of $E_\Lambda^{\rm eff}$ and $E_U^{\rm eff}$ are assumed to be the same in the considered (q,U) planes for magnetic field lines which intersect the 300-km altitude at geomagnetic latitudes $\varphi \geq \varphi_A$. The equatorial effective electric fields $E_\Lambda^{\rm eff}$ and $E_U^{\rm eff}$ are used for magnetic field lines, which intersect the geomagnetic equatorial points at the geomagnetic equatorial crossing heights $h_{eq}^k \leq 500$ km. Linear interpolation of the equatorial and Arecibo quantities of $E_\Lambda^{\rm eff}$ and $E_U^{\rm eff}$ are employed at intermediate dipole magnetic field lines.

The finite-difference algorithm described above yields approximations to N_i, N_e, T_i, and T_e in the ionosphere and plasmasphere at 72 Eulerian computational grid (q,U) planes with the time step Δt=10 min. The interpolation procedure is used to find the values of N_i, N_e, T_i, and T_e at points which are located between 72 Eulerian computational grid (q,U) planes. Using initial ion densities, and electron and ion temperatures, the model is run from 14:00 UT on 10 April 1958 to 24:00 UT on 13 April 1958. To neglect the effects of the initial conditions on N_i, T_i, and T_e, the values of N_i, T_i, and T_e produced by the model from 14:00 UT on 10 April 1958 to 24:00 UT on 11 April 1958 are not taken into consideration, and the model results are used during the studied time period from 00:00 UT on 12 April 1958 to 24:00 UT on 13 April 1958. As the model inputs, the horizontal components of the neutral wind are specified using the HWM90 wind model (Hedin et al., 1991), the model solar EUV fluxes are taken from the EUVAC model (Richards et al., 1994), while neutral densities and temperature are taken from the NRLMSISE-00 model (Picone et al., 2002).

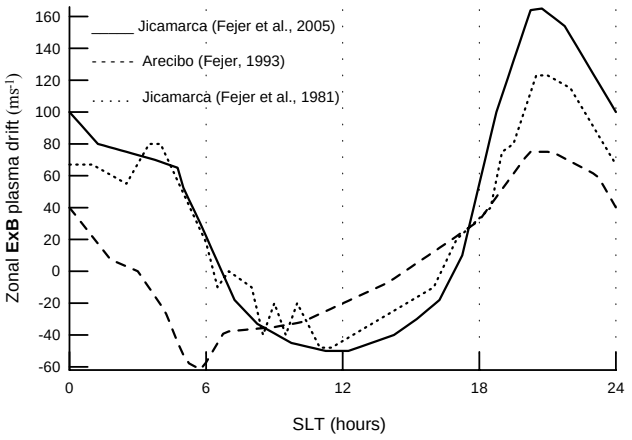

Fig. 2. Diurnal variations of the quiet time zonal $\boldsymbol{E}\times\boldsymbol{B}$ plasma drift velocity at F-region altitudes over Jicamarca (solid and dotted lines) and over Arecibo (dashed line) for equinox conditions at solar maximum. The Jicamarca zonal $\boldsymbol{E}\times\boldsymbol{B}$ plasma drift velocity are taken from Fig. 2 of Fejer et al. (2005) (solid line) and from Fig. 2 of Fejer et al. (1981) (dotted line), while the dashed line represents the Arecibo data presented in Fig. 3 of Fejer (1993). The zonal $\boldsymbol{E}\times\boldsymbol{B}$ plasma drifts shown by the solid and dashed lines are used in the model simulations of this work (see Sect. 2), while the data presented by the dotted line were used by Anderson (1981) (see discussion in Sect. 4). SLT is the solar local time (SLT=UT+ψ/15, where ψ is the geographic latitude).

3 Solar geophysical conditions and data

The characteristic time of the neutral composition recovery after a storm impulse event ranges from 7 to 12 h, on average (Hedin, 1987), while it may need up to several days for all altitudes down to 120 km in the atmosphere to recover completely back to the undisturbed state of the atmosphere (Richmond and Lu, 2000). The value of the geomagnetic Kp index was in the range from 1_- to 3_0 during 10–11 April 1958 and between 0_+ and 3_- during 12–13 April 1958. Therefore, the studied time period of 12–13 April 1958 can be considered as a geomagnetically quiet time period. The F10.7 solar activity index was equal to 197 on 12 April and 181 on 13 April, while the 81-day averaged F10.7 solar activity index centered on 12 or 13 April was close to 244.

Hourly critical frequencies, *fo*F2 and *fo*E, of the F2 and E layers, and maximum usable frequency parameter, M(3000)F2, from the La Paz, Natal, Bombay, Ahmedabad, Trivandrum, Kodaikonal, Tiruchirapalli, Delhi, Calcutta, Singapore, Maui, Talara, Panama, Chiclayo, Huancayo, and Bogota ionospheric sounder stations, which are available at the Ionospheric Digital Database of the National Geophysical Data Center, Boulder, Colorado, are used as a base for the purpose of this investigation. The locations of these ionospheric sounder stations are shown in Table 1. The value of the peak density, *Nm*F2, of the F2 layer is related to the critical frequency *fo*F2 as $NmF2=1.24\times10^{10}\ foF2^2$, where the unit of *Nm*F2 is m^{-3}, the unit of *fo*F2 is MHz. To determine the ionosonde value of *hm*F2, the relation between *hm*F2 and the values of $M(3000)F2$, *fo*F2, and *fo*E recommended by Dudeney (1983) is used as $hmF2=1490/[M(3000)F2+\Delta M]-176$, where $\Delta M=0.253/(foF2/foE-1.215)-0.012$. If there are no *fo*E data, then it is suggested that $\Delta M=0$, i.e. the *hm*F2 formula of Shimazaki (1955) is used. The reliability of *hm*F2

Table 1. Ionosonde station names and locations, and the maximum model value of *Nm*F2/*Nm*F2(V_Λ^E=0) over each ionosonde station during 12–13 April 1958. Geomagnetic latitudes and longitudes are calculated in eccentric (first number) and centered (second number) dipole approximations for the geomagnetic field using the parameters of these magnetic field approximations for the time period 1958.

Ionosonde Stations	Geographic latitude	Geographic longitude	Geomagnetic latitude	Geomagnetic longitude	$[NmF2/NmF2(E_U=0)]_{max}$
La Paz	−16.5	291.9	−5.2, −5.0	3.4, 1.2	1.2
Natal	−5.3	324.9	3.5, 4.2	34.4, 34.2	1.2
Bombay	19.0	72.8	9.5, 9.8	140.1, 143.8	2.4
Ahmedabad	23.0	72.6	13.6, 13.8	140.3, 145.8	2.1
Trivandrum	8.5	77.0	−1.6, −1.1	143.0, 146.8	2.3
Kodaikonal	10.2	77.5	0.1, 0.5	143.7, 147.4	2.3
Tiruchirapalli	10.8	78.7	0.6, 1.0	144.9, 148.7	2.3
Delhi	28.6	77.2	18.8, 18.8	145.3, 149.2	1.5
Calcutta	23.0	88.6	12.2, 12.3	155.7, 159.3	2.2
Singapore	1.3	103.8	−11.1, −10.1	170.1, 173.0	2.1
Maui	20.8	203.5	21.4, 20.9	271.8, 268.4	1.1
Talara	−4.5	278.6	6.0, 6.8	350.8, 347.9	1.5
Panama	9.4	280.1	19.4, 20.7	351.9, 348.9	1.1
Chiclayo	−6.7	280.1	4.0, 4.6	352.3, 349.5	1.5
Huancayo	−12.0	284.6	−1.0, −0.6	356.7, 354.1	1.4
Bogota	4.5	285.8	14.8, 16.0	357.6, 355.0	1.2

derived from the observed values of $M(3000)$F2, *fo*F2, and *fo*E by means of the Dudeney (1983) approach is supported by the reasonable agreement between these values of *hm*F2 and those measured by the middle and upper atmosphere radar at Shigaraki (34.85° N, 136.10° E) during 19–21 March 1988 and 25–27 August 1987 (Pavlov et al., 2004a, b).

4 Model/data comparisons

The measured (squares) and calculated (lines) *Nm*F2 and *hm*F2 are displayed in Figs. 3–6 from 00:00 UT on 12 April to 24:00 UT on 13 April above the ionosonde stations presented in Table 1. For clarity, the solar local time, SLT, is used in Figs. 3–6 for each ionosonde station (SLT=UT+ψ/15, where ψ is the geographic latitude). The NRLMSISE-00 neutral temperature and densities, and the equatorial E_Λ given by the equatorial perpendicular plasma drift model of Scherliess and Fejer (1999) for the studied time period are used in producing the model results shown by dashed lines in Figs. 3–6. Solid and dotted lines show the results from the model with the corrected E_Λ and NRLMSISE-00 atomic oxygen density, which are discussed below. The zonal component of the plasma drift described in Sect. 2 is taken into account in the model results shown by solid and dashed lines in Figs. 3–6, while dotted lines in Figs. 3–6 are produced by the model when the zonal plasma drift is equal to zero.

Close to the geomagnetic equator, the meridional wind has little effect on the spatial and temporal features of the distribution of plasma, and the meridional $\boldsymbol{E}\times\boldsymbol{B}$ plasma drift is the primary force in determining *hm*F2 (Rishbeth, 2000; Souza et al., 2000; Pavlov, 2003; Pavlov et al., 2004a, b). As a result, it is necessary to compare the measured and modeled *hm*F2 close to the geomagnetic equator to adjust the value of E_Λ for the studied time period. The comparison between the measured *hm*F2 shown by the squares in Figs. 3–6 and the calculated *hm*F2 shown by the dashed lines in Figs. 3–6 clearly indicates that there is a large disagreement between the measured and modeled *hm*F2 over the Natal, Ahmedabad, Talara, and Chiclayo ionosonde stations close to 18:00–20:00 SLT on 12 and 13 April 1958 if the equatorial E_Λ determined by the plasma drift model of Scherliess and Fejer (1999) is used. It follows from the model simulations that it is unlikely to make the measured and modeled *hm*F2 over these ionosonde stations agree via changes in the neutral wind, densities, and temperature. The model of the ionosphere and plasmasphere overestimates *hm*F2 under conditions of strong upward plasma drifts before and during the evening prereversal plasma drift enhancement, transporting ions and electrons from lower to higher altitudes. Therefore, if the equatorial perpendicular plasma drift given by the empirical model of Scherliess and Fejer (1999) at each geomagnetic longitude over the geomagnetic equator exceeds 20 ms^{-1} from 16:00 SLT to 20:00 SLT, then it is set to 20 ms^{-1}, to improve the agreement between the measured and modeled *hm*F2 over the Natal, Ahmedabad, Talara, and Chiclayo ionosonde stations.

Figures 3–6 show that the modeled daytime values of *Nm*F2, given by dashed lines, are overestimated in comparison with the observed values. It can be expected that the

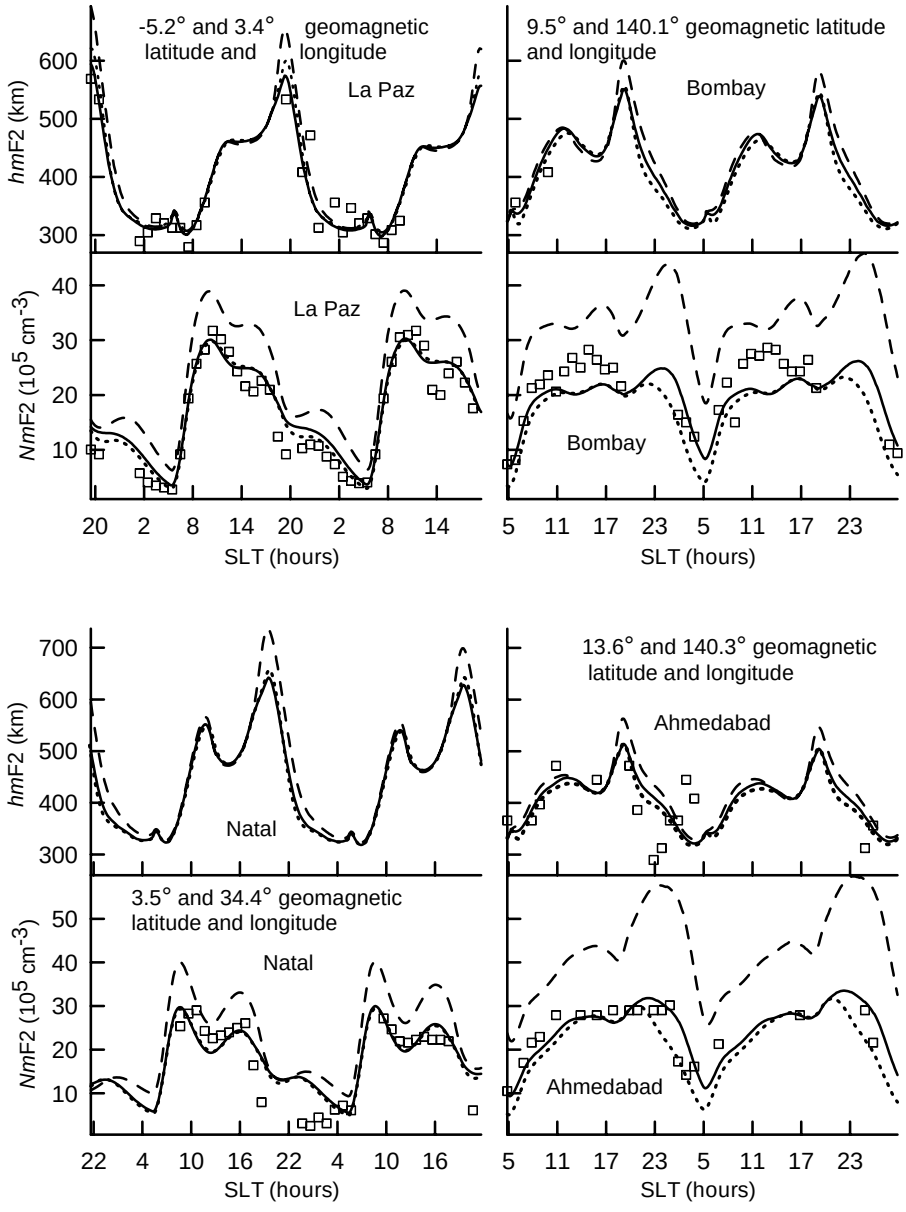

Fig. 3. Observed (squares) and calculated (lines) *Nm*F2 and *hm*F2 above the La Paz, Natal, Bombay, and Ahmedabade ionosonde stations from 00:00 UT on 12 April 1958 to 24:00 UT on 13 April 1958. SLT is the solar local time at each ionosonde station. The results obtained from the model of the ionosphere and plasmasphere using the equatorial E_Λ, produced by the equatorial perpendicular plasma drift model of Scherliess and Fejer (1999), and the NRLMSISE-00 neutral temperature and densities, as the input model parameters, are shown by dashed lines. Solid and dotted lines show the results given by the model with the corrected equatorial E_Λ and the NRLMSISE-00 model with the corrected value of [O]. The corrected meridional $\boldsymbol{E}\times\boldsymbol{B}$ plasma drift given by the model of Scherliess and Fejer (1999) is taken to be 20 ms^{-1} from 16:00 SLT to 20:00 SLT at each geomagnetic longitude over the geomagnetic equator, if this drift is larger than 20 ms^{-1}. The NRLMSISE-00 model atomic oxygen number density was decreased by a factor of C in the both hemispheres at all times and altitudes. The value of C is found to be 1.5 at all geomagnetic latitudes, if the geomagnetic longitude is located between 140° and 155°. In the geomagnetic longitude ranges from 0° to 35° and from 350° to 360°, the [O] correction factor is estimated to be 1.5 at geomagnetic latitudes exceeding 15° and below −15°, C=1.2 at the geomagnetic equator, and the value of C decreases linearly from 1.5 to 1.2, if the geomagnetic latitude is changed from −15° to 0° and from 15° to 0°. The [O] correction factor varies linearly in geomagnetic longitude between 35° and 140° and from 155° and to 350°, if the value of the geomagnetic latitude is not changed. The zonal $\boldsymbol{E}\times\boldsymbol{B}$ plasma drift described in Sect. 2 is taken into account in the model results shown by solid and dashed lines, while dotted lines are produced by the model when the zonal plasma drift is equal to zero.

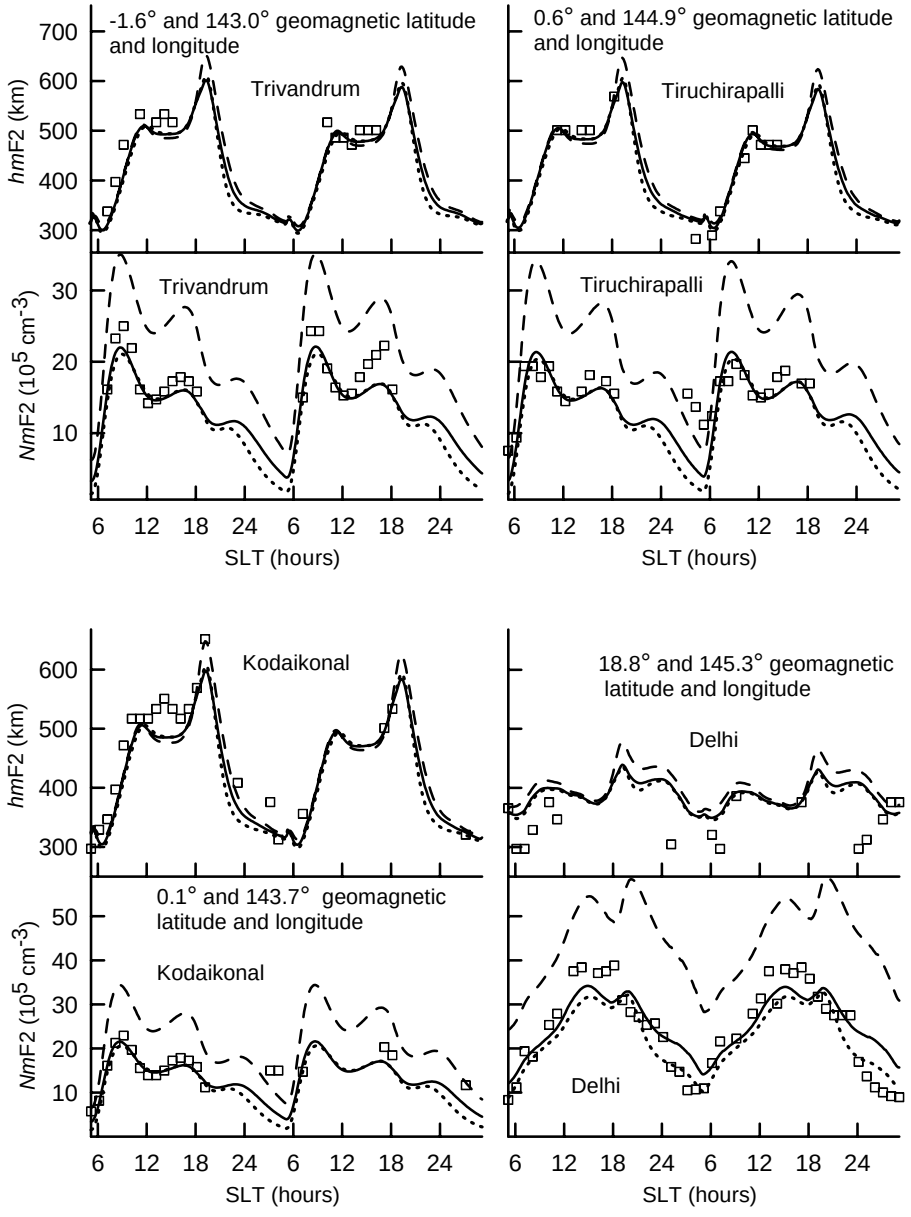

Fig. 4. From bottom to top, observed (squares) and calculated (lines) of *Nm*F2 and *hm*F2 above the Trivandrum, Kodaikonal, Tiruchirapalli, and Delhi ionosonde stations during 12–13 April 1958. SLT is the solar local time at each ionosonde station. The curves are the same as in Fig. 3.

NRLMSISE-00 model has some inadequacies in predicting the number densities with accuracy. This model assumes the use of the analytical formula to calculate the neutral density altitude profiles at altitudes above 120 km by integrating the equation of diffusion equilibrium given as

$$\frac{\partial}{\partial z}\ln n_n + H_n^{-1} + (1+\alpha_n)\frac{\partial}{\partial z}\ln T_n = 0, \quad (4)$$

where n_n denotes a number density of the n-th neutral component, z is an altitude, H_n=kT_n $(m_n g)^{-1}$, k is Boltzmann's coefficient, m_n denotes the mass of the n-th neutral component, g is the acceleration due to gravity, α_n is a thermal diffusion coefficient.

The NRLMSISE-00 neutral temperature profile is calculated above the 120-km altitude as

$$T_n(z)=T_\infty-[T_\infty-T_n(z_0)]\exp[-\sigma(z-z_0)(R_E+z_0)/(R_E+z)], \quad (5)$$

where T_∞ is an exospheric temperature, z_0=120 km, and σ is a shape factor.

The value of $n_n(z)$ produced by the NRLMSISE-00 model is a function of $n_n(z_0)$, T_∞, $T_n(z_0)$, and σ determined by Picone et al. (2002) from measurements of the

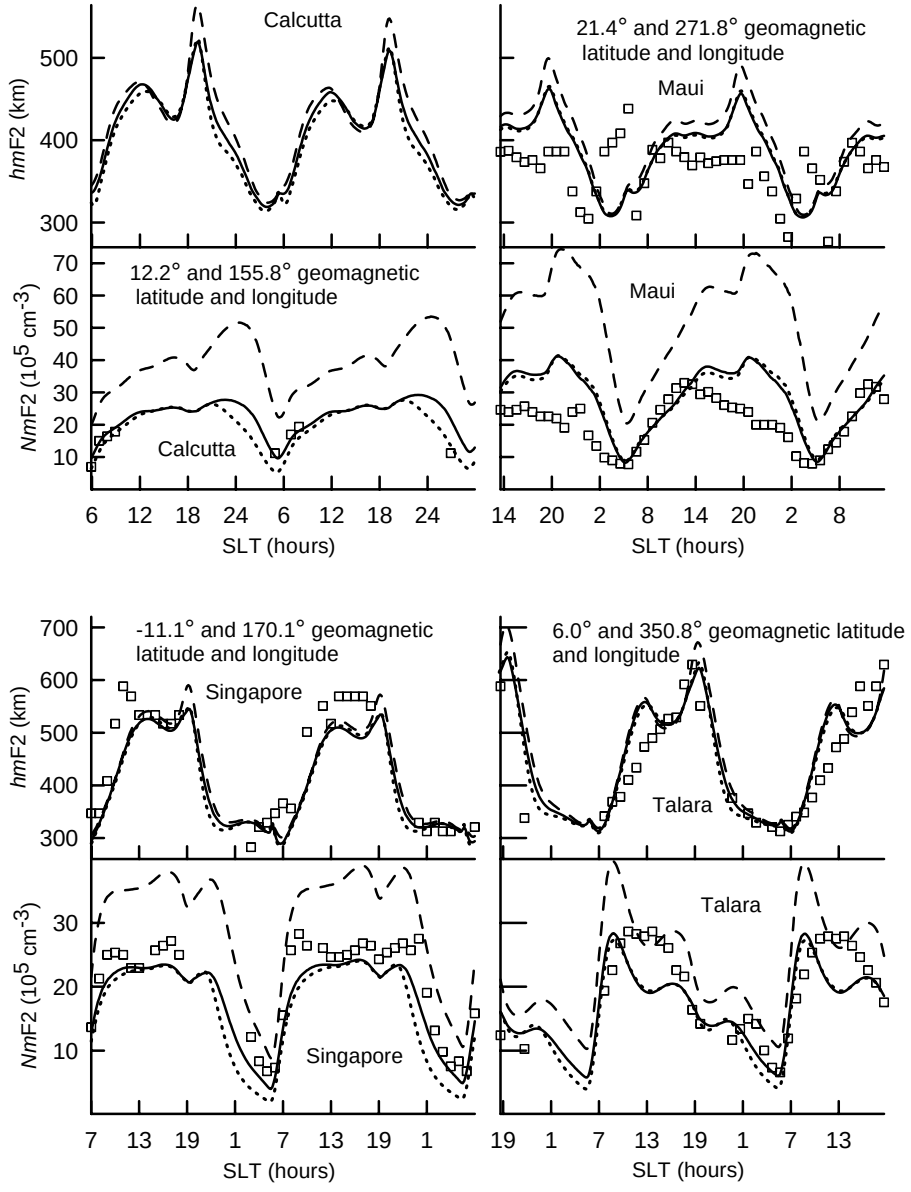

Fig. 5. From bottom to top, observed (squares) and calculated (lines) of *Nm*F2 and *hm*F2 above the Calcutta, Singapore, Maui, and Panama ionosonde stations during 12–13 April 1958. SLT is the solar local time at each ionosonde station. The curves are the same as in Fig. 3.

neutral temperature and densities, i.e. inaccuracies in the NRLMSISE-00 neutral temperature and number densities can arise from inaccuracies in the predictions of $n_n(z_0)$, T_∞, $T_n(z_0)$, and σ. Unfortunately, Picone et al. (2002) did not publish statistical distributions of data used by the NRLMSISE-00 model in time, in altitude, in months, in latitude, in longitude, and in solar and geomagnetic activities. Nevertheless, it is possible to suppose that, as a result of a limited amount of measurements of $n_n(z)$ and $T_n(z)$, not all geophysical conditions are well represented in this model. Errors in satellite and rocket measurement of $n_n(z)$ and $T_n(z)$ used by the NRLMSISE-00 model as the base data set also make a contribution to the inaccuracies of the calculated NRLMSISE-00 $n_n(z)$ and $T_n(z)$.

Lean et al. (2006) have analyzed the total mass density of the atmosphere measured by three Starshine spacecraft at altitudes between 200 and 475 km at solar maximum and have found larger differences of as much as 30% between the measured total mass density and that produced by the NRLMSISE-00 model which can persist on time scales of several months. A part of this inaccuracy in the NRLMSISE-00 model prediction is reduced if an improved solar EUV irradiance index, such as the Mg II index, is used as the input parameter of the NRLMSISE-00 model instead of the solar

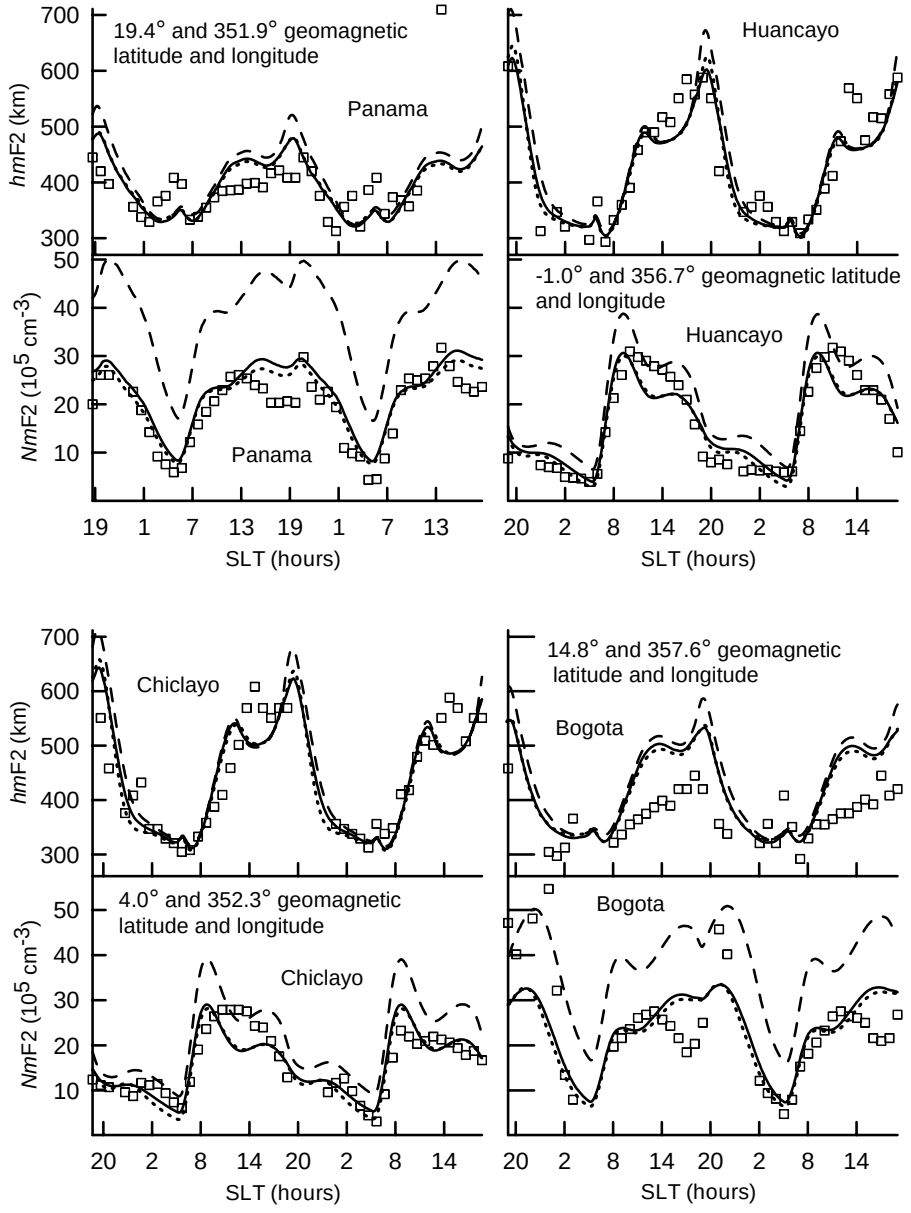

Fig. 6. From bottom to top, observed (squares) and calculated (lines) of *Nm*F2 and *hm*F2 above the Talara, Chiclayo, Huancayo, and Bogota ionosonde stations during 12–13 April 1958. SLT is the solar local time at each ionosonde station. The curves are the same as in Fig. 3.

10.7 cm radio flux (Lean et al., 2006). It was pointed out by Lean et al. (2006) that the total mass densities given by the NRLMSIS-00 model underestimate the upper atmosphere response associated with solar 27-day rotational modulation of EUV radiation seen in the Starshine drag densities, up to a factor of two. In the lower thermosphere, the primary source of information on [O] is the mass spectrometer data on a sum of [O] and 2[O_2] (Picone et al., 2002), and it may be a source of inaccuracies in [O] produced by the NRLNSISE-00 model. It is worth noting that above about 127 km, diffusion becomes dominant over photochemistry for O, but diffusive equilibrium is not fully established until about 166 km, and in some places even higher (Rishbeth and Müller-Wodarg, 1999). Models such as NRLMSISE-00 generally assume that diffusive equilibrium exists above 120 km, but this assumption may introduce errors of 25% or more in model values of [O]/[N_2] at F2-layer heights for quiet geomagnetic conditions (Rishbeth and Müller-Wodarg, 1999).

It is necessary to modify the NRLMSISE-00 number densities to bring the modeled electron densities into better agreement with the measurements (see Figs. 3–6). As a result, the value of [O] was decreased by a factor of C in both hemispheres at all times and altitudes from the comparison between the modeled *Nm*F2 and *Nm*F2 measured by the

ionosonde stations of Table 1. It is found from the model simulations that C=1.5 at all geomagnetic latitudes, if the geomagnetic longitude is changed between 140° and 155°. In the geomagnetic longitude ranges from 0° to 35° and from 350° to 360°, the value of C is estimated to be 1.5 at geomagnetic latitudes exceeding 15° and below −15°, C=1.2 is taken at the geomagnetic equator, and the [O] correction factor decreases linearly from 1.5 to 1.2 if the geomagnetic latitude is changed from −15° to 0° and from 15° to 0°. The [O] correction factor varies linearly in geomagnetic longitude between 35° and 140° and from 155° and to 350°, if the value of the geomagnetic latitude is not changed. This correction of the NRLMSISE-00 atomic oxygen number density is used in the model results presented in Sect. 5.

It should be noted that the values of *Nm*F2 and *hm*F2 and the model results and conclusions described in Sects. 5 and 6 are practically not sensitive to the above-mentioned correction of the NRLMSISE-00 atomic oxygen number density by night, and the night-time correction of [O] is employed to avoid sharp changes in [O] between daytime and night-time conditions. On the other hand, during daytime periods the value of *Nm*F2 is approximately proportional to [O]/L(O^+), where L(O^+) is the loss rate of $O^+(^4S)$ ions in the reactions of these ions with vibrationally unexcited and vibrationally excited molecular nitrogen and oxygen, described in detail by Pavlov (1998). It means that it is possible to make a comparable agreement between the measured and modeled daytime *Nm*F2 by decreasing [O] by a correction factor of C, or by increasing the daytime values of [N_2] and [O_2] by the same correction factor of C, or decreasing [O] and increasing [N_2] and [O_2] by day, so that the [O]/[N_2] and [O]/[O_2] ratios are decreased by the same correction factor of C. This conclusion is supported by the model simulations. It is worth noting that the value of *Nm*F2 is a function of L(O^+) by night and the use of the above-mentioned correction in [N_2] and [O_2] as an alternative of the correction in [O] is limited by daytime conditions. It is found from the model simulations that the model which uses these different neutral density corrections with the same correction factor of C produces close results, and the validity of the main results of this work is not dependent on the alternative choice of the neutral density corrections.

Solid and dotted lines in Figs. 3–6 show the results given by the model, which uses the corrected equatorial E_Λ and the modified NRLMSISE-00 [O] described above. One can see from the comparison between the squares and the solid lines in Figs. 3–6 that these modifications of E_Λ and [O] bring the measured and modeled *Nm*F2 and *hm*F2 into better agreement.

Figures 3–6 show that there are some quantitative differences between the measured *Nm*F2 and *hm*F2 and those shown by solid lines. These differences can be the result of scattering in the data caused by measurement errors, and can be produced by considerable day-to-day variability in the equatorial electrojet (Rishbeth, 2000). It should be noted that the Jicamarca vertical $\boldsymbol{E}\times\boldsymbol{B}$ plasma drifts are most variable over a period of about 4 weeks, centered on the equinox (Fejer and Scherliess, 2001). The empirical model of Scherliess and Fejer (1999) was created by averaging a great deal of data to find the mean trends in noisy data and create smooth curves. Therefore, the equatorial meridional drift patterns produced by this model describe only average diurnal changes in the equatorial meridional drift (see very large scattering in the measured vertical plasma drift in Figs. 1 and 2 of Scherliess and Fejer, 1999). It is possible to assume that there are differences in longitude of this day-to-day variability in E_Λ, which is not used by the model. It is also possible that the NRLMSISE-00 [O] correction factor is inconstant in time, and the NRLMSISE-00 model has some inadequacies in predicting the actual [N_2] and [O_2] with accuracy for the studied time period. A possible difference between the HWM90 wind and the real wind for the studied time period can also produce a part of some quantitative differences between the measured and modeled *Nm*F2 and *hm*F2. Nevertheless, the use of the corrected [O] and E_Λ brings the measured and modeled *Nm*F2 and *hm*F2 into reasonable agreement, which is enough to carry out the study of the influence of the zonal $\boldsymbol{E}\times\boldsymbol{B}$ plasma drift on N_e.

5 Effect of the zonal $\boldsymbol{E}\times\boldsymbol{B}$ plasma drift on N_e

It is evident from the comparison between the solid and dotted lines in Figs. 3–6 that V_Λ^E produces small effects in *Nm*F2 during the daytime periods, the zonal $\boldsymbol{E}\times\boldsymbol{B}$ plasma drift gives rise to a considerable increase in *Nm*F2 during the night-time period, and there is the tendency for the influence of V_Λ^E on *Nm*F2 to peak after midnight. The influence of the zonal $\boldsymbol{E}\times\boldsymbol{B}$ plasma drift on *Nm*F2 and *hm*F2 is characterized by the *Nm*F2/*Nm*F2(V_Λ^E=0) ratio and the *hm*F2–*hm*F2(V_Λ^E=0) difference, where *Nm*F2(V_Λ^E=0) and *hm*F2(V_Λ^E=0) are the F2-layer peak density and altitude produced by the model, which does not include the zonal $\boldsymbol{E}\times\boldsymbol{B}$ plasma drift. The maximum *Nm*F2/*Nm*F2(V_Λ^E=0) ratio over the ionosonde stations is presented in Table 1.

The two low panels of Fig. 7 show the maximum model value of *Nm*F2/*Nm*F2(V_Λ^E=0) during 12–13 April 1958 at the geomagnetic latitudes of 0°, −10°, −20° (the solid, dashed, and dotted lines in the panel (a), respectively) and 10°, 20° (the solid and dashed in the panel (b), respectively). The longitudinal changes in the *Nm*F2/*Nm*F2(V_Λ^E=0) ratio over the geomagnetic equator at 20:00 SLT (dashed line), and 24:00 SLT (solid line) shown in the panel (d) of Fig. 6, and the maximum model value of $N_e/N_e(V_\Lambda^E=0)$ over the geomagnetic equator at 700 km (solid line), 1000 km (dashed line), and 1500 km (dotted line), shown in the top panel of Fig. 7, are discussed later in this section. The model results show that there are significant differences in $[Nm\text{F2}/Nm\text{F2}(V_\Lambda^E=0)]_{\max}$ at different geomagnetic latitudes and longitudes. The main peak value of

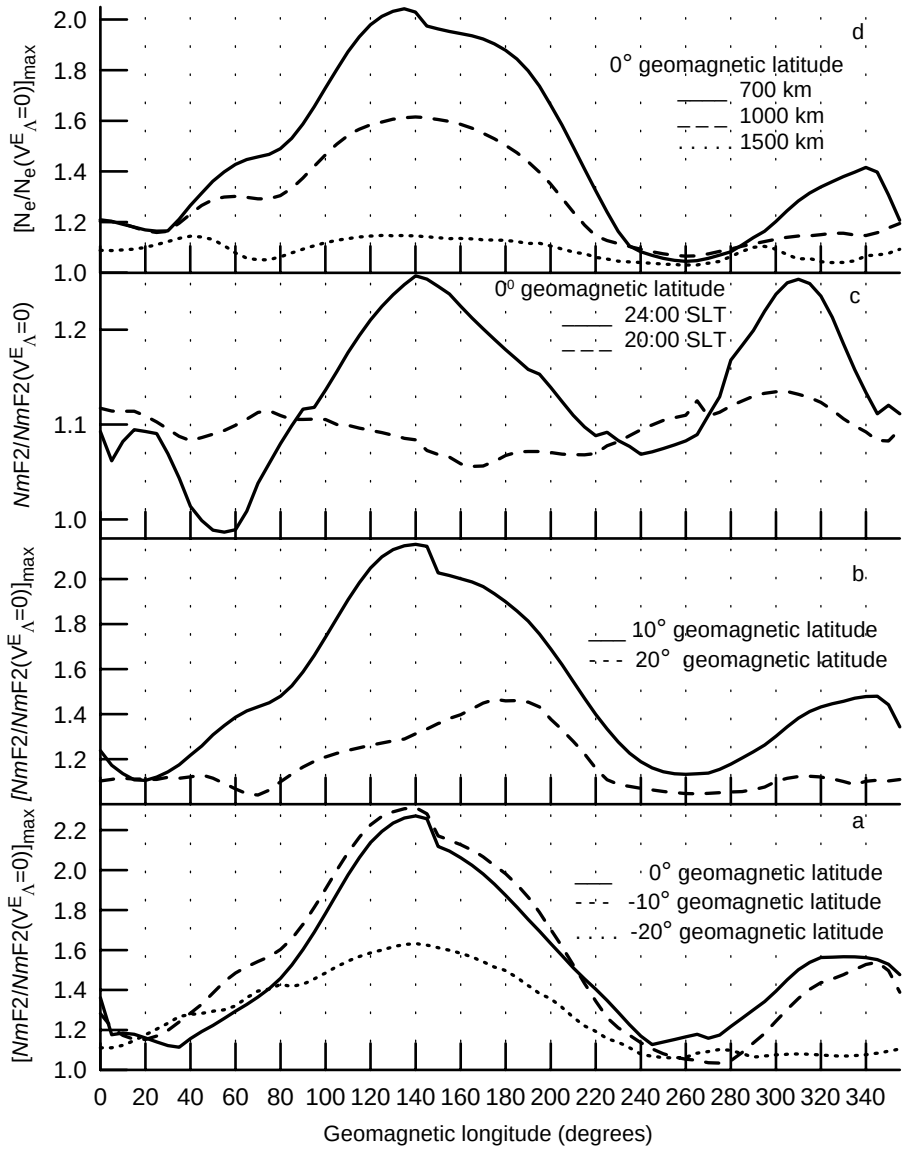

Fig. 7. The maximum model value of NmF2/NmF2(V^E_Λ=0) during 12–13 April 1958 at the geomagnetic latitudes of 0° (solid line in the panel **a**), −10° (dashed line in the panel a), −20° (dotted line in the panel a), 10° (solid line in the panel **b**), and 20° (dashed line in the panel b). The panel **(c)** shows the longitudinal changes of the NmF2/NmF2(V^E_Λ=0) ratio over the geomagnetic equator at 20:00 SLT (dashed line) and 24:00 SLT (solid line) on 12 April 1958. The panel **(d)** shows the maximum ratio of the calculated electron density over the geomagnetic equator to that obtained when the zonal $\boldsymbol{E}\times\boldsymbol{B}$ drift is omitted at 700 km (solid line), 1000 km (dashed line), and 1500 km (dotted line).

$[Nm\text{F2}/Nm\text{F2}(V^E_\Lambda=0)]_{\max}$ is estimated from the numerical simulations to be 2.15–2.31 between −10° and 10° geomagnetic latitude at 140° geomagnetic longitude, and this main peak is less pronounced at −20° and 20° geomagnetic latitudes, in comparison with that between −10° and 10° geomagnetic latitude. The $[Nm\text{F2}/Nm\text{F2}(V^E_\Lambda=0)]_{\max}$ ratio is found to be 1.04–1.20 at 20° geomagnetic latitude from 0° to 95° and from 220° to 360° geomagnetic longitude, while $[Nm\text{F2}/Nm\text{F2}(V^E_\Lambda=0)]_{\max}$=1.06–1.20 at −20° geomagnetic latitude from 0° to 25° and from 220° to 360° geomagnetic longitude. The two low panel of Fig. 7 show that the model also produces the second peak in $[Nm\text{F2}/Nm\text{F2}(V^E_\Lambda=0)]_{\max}$ between −10° and 10° geomagnetic latitude, which is equal to 1.48–1.57 and located from 330° to 345° geomagnetic longitude. As a result, the present study provides first evidence that there are longitude sectors where the enhancements in NmF2 due to the zonal $\boldsymbol{E}\times\boldsymbol{B}$ plasma drift are more pronounced. A noticeable feature of the change in $Nm\text{F2}/Nm\text{F2}(V^E_\Lambda=0)]_{\max}$ in geomagnetic longitude is its local minimums in the 1.03–1.15 range, which are formed at

20–35° geomagnetic longitudes and at 245–275° geomagnetic longitudes between −10° and 10° geomagnetic latitude. Hence, this work provides first evidence that the influence of the zonal $\boldsymbol{E}\times\boldsymbol{B}$ plasma drift on *Nm*F2 is less pronounced close to the above-mentioned geomagnetic longitude, where local minimums of $[NmF2/NmF2(V_\Lambda^E=0)]_{max}$ are formed. The influence of the zonal $\boldsymbol{E}\times\boldsymbol{B}$ plasma drift on *Nm*F2 is feebly marked ($[NmF2/NmF2(V_\Lambda^E=0)]_{max}\leq 1.1$) and can be neglected between 55° and 95° geomagnetic longitude, between 230° and 300° geomagnetic longitude, and from 330° to 350° geomagnetic longitude at 20° geomagnetic latitude, and in the 240–355° geomagnetic longitude range at −20° geomagnetic latitude. The difference between the calculated F2-peak altitude and that obtained when the zonal $\boldsymbol{E}\times\boldsymbol{B}$ drift is omitted is inessential ($|hmF2-hmF2(V_\Lambda^E=0)|\leq 10$ km) at −20° and at 20° geomagnetic latitude between 0° and 105° geomagnetic longitude and from 210° to 360° geomagnetic longitude. By comparing the solid and dashed lines in Fig. 2, it is seen that the night-time eastward drift over the geomagnetic equator is considerably larger than the night-time eastward drift over Arecibo. As a result of this weakening of the night-time eastward drift in geomagnetic latitude, the influence of the zonal $\boldsymbol{E}\times\boldsymbol{B}$ plasma drift on *Nm*F2 and *hm*F2 is found to be negligible above about 25° and below about −26° geomagnetic latitude at all geomagnetic longitudes ($[NmF2/NmF2(V_\Lambda^E=0)]_{max}\leq 1.09$ and $|hmF2-hmF2(V_\Lambda^E=0)|\leq 5$ km at −26° and 25° geomagnetic latitude).

After sunset, the daytime F2-region decay is caused by $O^+(^4S)$ ion losses with a rate in chemical reactions of $O^+(^4S)$ ions with vibrationally unexcited and excited N_2 and O_2. Field-aligned diffusion of ions and electrons transport ionization from the topside ionosphere to F2-region altitudes maintaining night-time *Nm*F2. The night-time gain of ionization at the F2-peak is caused by the meridional $\boldsymbol{E}\times\boldsymbol{B}$ drift, which is directed from higher L-shells to lower L-shells. The plasma drift along magnetic field lines due to neutral winds modulates the night-time *Nm*F2 in a constructive or destructive manner, depending upon the direction of the meridional wind. A poleward meridional wind causes a lowering of the F2-region height and a resulting reduction in *Nm*F2 due to an increase in the loss rate of $O^+(^4S)$ ions, whereas a meridional wind, which is equatorwards, tends to increase the value of *Nm*F2 by transporting the plasma up along field lines to regions of lower chemical loss of $O^+(^4S)$ ions. These processes lead to a dependence of *Nm*F2 on SLT by night, forming *Nm*F2 changes in geomagnetic longitude at fixed values of altitude and geomagnetic latitude. In addition to the above-mentioned processes, the plasma moves in longitude by the strong eastward zonal $\boldsymbol{E}\times\boldsymbol{B}$ drift velocity, creating an additional source of electron and ions, so that the night-time plasma density is maintained above values which would be calculated in the absence of this eastward drift and the above-mentioned processes can modulate the effect of the zonal $\boldsymbol{E}\times\boldsymbol{B}$ drift on N_e. If the meridional $\boldsymbol{E}\times\boldsymbol{B}$ plasma drift at 0° geomagnetic longitude and zero neutral wind are employed at all geomagnetic longitudes, and a centered dipole approximation for the geomagnetic field (the Earth's centric tilted magnetic dipole moment is inclined with respect to the Earth's rotational axis) is used, then the model produces feebly marked variations of $[NmF2/NmF2(V_\Lambda^E=0)]_{max}$ in geomagnetic longitude. For example, if Λ=0–360°, then $[NmF2/NmF2(V_\Lambda^E=0)]_{max}$=1.90–2.05 over the geomagnetic equator, and $[NmF2/NmF2(V_\Lambda^E=0)]_{max}$=1.88–2.00 and 1.90–1.97 at −15° and 15° geomagnetic latitude, respectively. As a result of the model simulations, three major causes of the calculated longitude variations in $[NmF2/NmF2(V_\Lambda^E=0)]_{max}$ were revealed: (1) the longitudinal asymmetry in $\boldsymbol{B}$ (the eccentric magnetic dipole is displaced from the Earth's center and the Earth's eccentric tilted magnetic dipole moment is inclined with respect to the Earth's rotational axis), (2) the variations of the wind induced plasma drift in geomagnetic longitude caused by the changes in the displacement of the geomagnetic and geographic equators and the magnetic declination angle in geomagnetic longitude, and (3) the variations of the meridional $\boldsymbol{E}\times\boldsymbol{B}$ plasma drift in geomagnetic longitude (due to the longitudinal dependence of the meridional equatorial $\boldsymbol{E}\times\boldsymbol{B}$ plasma drift produced by the empirical model of Scherliess and Fejer, 1999).

In the topside night-time ionosphere, an increase in N_e caused by the zonal $\boldsymbol{E}\times\boldsymbol{B}$ plasma drift is transported from lower to higher altitudes by plasma diffusion along magnetic field lines, and, simultaneously, this increase in N_e is redistributed between magnetic field lines by the meridional $\boldsymbol{E}\times\boldsymbol{B}$ drift. As a result, the altitude dependence of the influence of V_Λ^E on N_e in the topside ionosphere over the geomagnetic equator is a function of changes in the effect of V_Λ^E on *Nm*F2 and *hm*F2 in geomagnetic latitude. As the top panel of Fig. 7 shows, the maximum effect of V_Λ^E on N_e decreases in altitude in the night-time topside ionosphere above 700 km over the geomagnetic equator and this effect is not significant above about 1500 km. The model simulations show that at 1000 km altitude the maximum $N_e/N_e(V_\Lambda^E=0)$ ratio is changed between 1.07 and 1.46 at −10° and 10° geomagnetic latitude and is found to be negligible at −20° and 20° geomagnetic latitude.

Shown in Figs. 8, 9, and 10 are plots of solar local time variations of the modeled values of $NmF2/NmF2(V_\Lambda^E=0)$, $hmF2-hmF2(V_\Lambda^E=0)$, and $N_e^{-1}\frac{\partial}{\partial\Lambda}N_e$ at *hm*F2 over the geomagnetic latitude of −15° (solid lines), 0° (dotted lines), and 15° (dashed lines) at the geomagnetic longitude of 0°, 45°, 90°, 135°, 180°, 225°, 270°, and 315°.

It follows from the model simulations that $0.96\leq NmF2/NmF2(V_\Lambda^E=0)\leq 1.1$ from about 07:55 SLT to about 19:47 SLT over the geomagnetic equator at all geomagnetic longitudes, and from about 08:32 SLT to about 22:00 SLT at −10° and 10° geomagnetic latitude at all geomagnetic longitudes. Thus, the enhancements in *Nm*F2 caused by the zonal $\boldsymbol{E}\times\boldsymbol{B}$ plasma drift are pronounced during

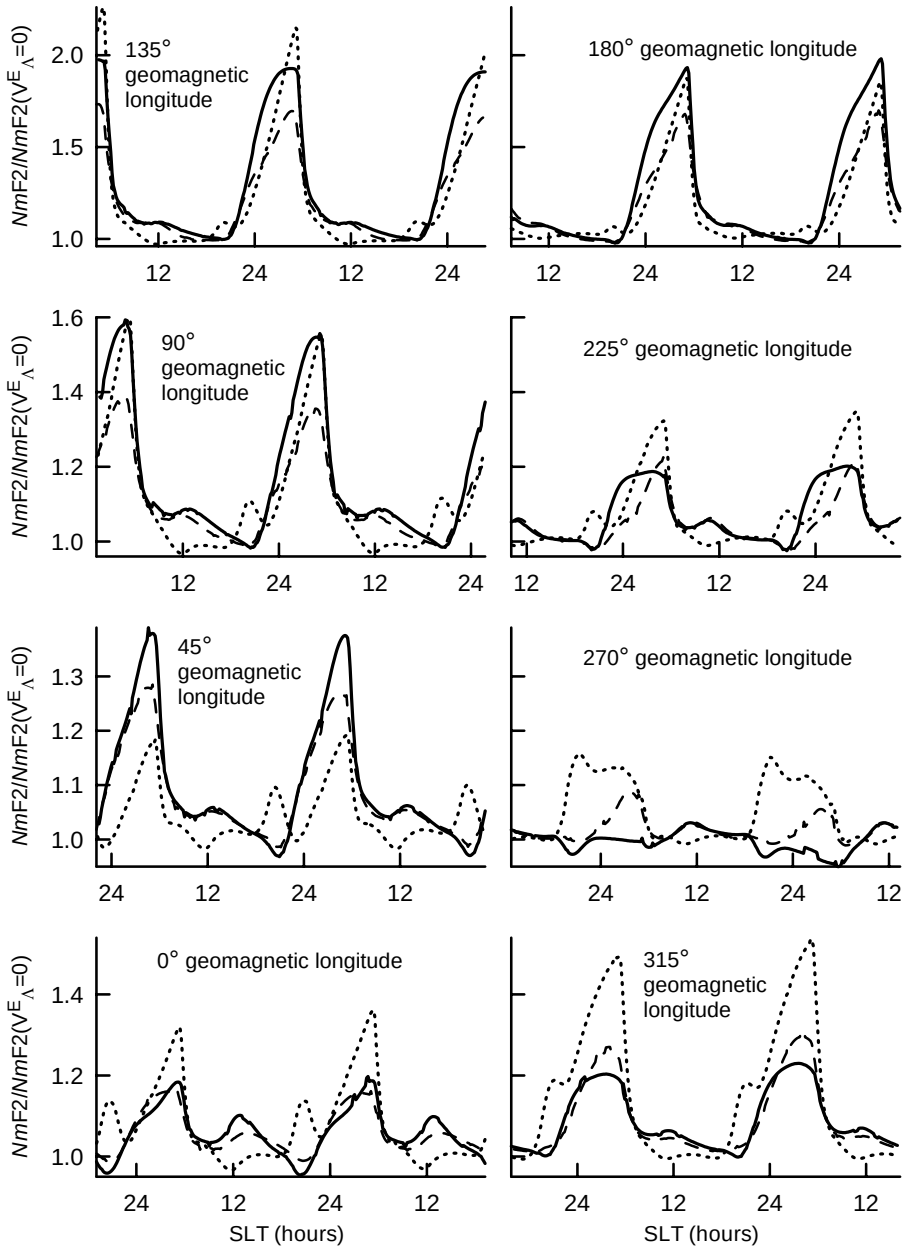

Fig. 8. The modeled *Nm*F2/*Nm*F2(V^E_Λ=0) ratio as a function of SLT from 00:00 UT on 12 April 1958 to 24:00 UT on 13 April 1958 over the geomagnetic latitude of $-15°$ (solid lines), 0° (dotted lines), and 15° (dashed lines) at the geomagnetic longitudes of 0°, 45°, 90°, 135°, 180°, 225°, 270°, and 315°.

a part of the night-time period, and changes in *Nm*F2 due to the zonal $\boldsymbol{E}\times\boldsymbol{B}$ plasma drift are hardly distinguished by day. As Fig. 9 shows, the difference between the calculated F2-peak altitude and that obtained when the zonal $\boldsymbol{E}\times\boldsymbol{B}$ drift is omitted is not significant in the daytime low-latitude ionosphere.

There are distinguishing features in the diurnal variations of $N_e^{-1}\frac{\partial}{\partial\Lambda}N_e$ at *hm*F2 presented in Fig. 10. These variations show a morning maximum caused by a sharp increase in *Nm*F2 after sunrise. During most of the daytime period the meridional $\boldsymbol{E}\times\boldsymbol{B}$ drift lifts the plasma from lower field lines to higher field lines, while during most of the night-time period this drift moves ions and electrons from higher field lines to lower field lines. Simultaneously, the plasma diffuses along the magnetic field lines. As a result of the morning reversal of the meridional $\boldsymbol{E}\times\boldsymbol{B}$ plasma drift, ions and electrons begin to move from lower L-shells to higher L-shells under the action of this drift, causing a drop in *Nm*F2 around the geomagnetic equator and a gain in ionization at F2-peak altitudes at higher geomagnetic latitudes, leading

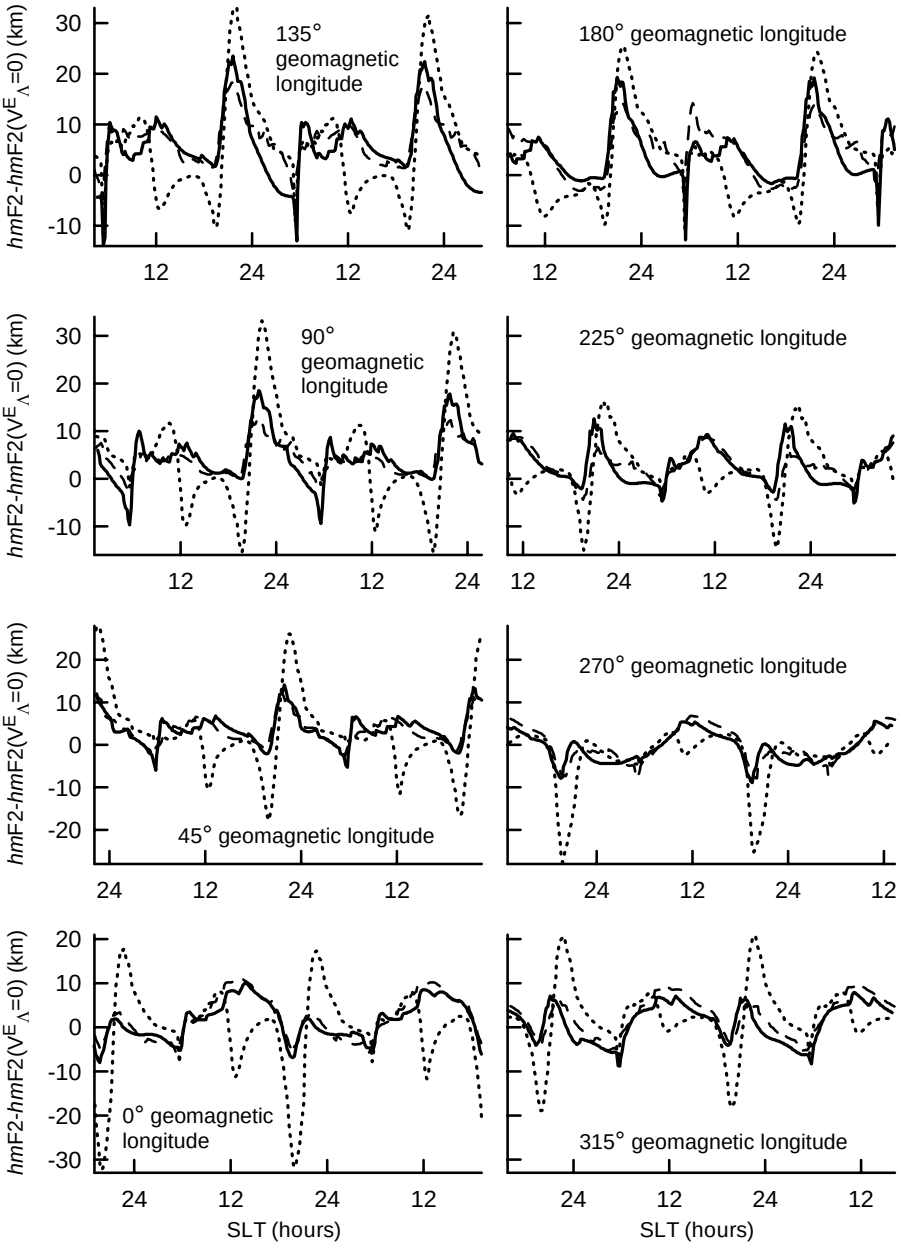

Fig. 9. The modeled *hm*F2–*hm*F2(V^E_Λ=0) difference as a function of SLT from 00:00 UT on 12 April 1958 to 24:00 UT on 13 April 1958 over the geomagnetic latitude of −15° (solid lines), 0° (dotted lines), and 15° (dashed lines) at the geomagnetic longitudes of 0°, 45°, 90°, 135°, 180°, 225°, 270°, and 315°.

to the formation of the equatorial anomaly. These physical processes are responsible for the formation of a local minimum in $N_e^{-1}\frac{\partial}{\partial\Lambda}N_e$ before 12:00 SLT over the geomagnetic equator. For the same reasons, the presence of a local evening minimum in $N_e^{-1}\frac{\partial}{\partial\Lambda}N_e$ over the geomagnetic equator is explained by the evening pre-reversal enhancements of meridional $\boldsymbol{E}\times\boldsymbol{B}$ plasma drift produced by the Scherliess and Fejer (1999) model. After sunset, a decay in the daytime ionosphere leads to a decrease in *Nm*F2 and to a decrease in $N_e^{-1}\frac{\partial}{\partial\Lambda}N_e$, strengthening the influence of the zonal $\boldsymbol{E}\times\boldsymbol{B}$ plasma drift on *Nm*F2. Furthermore, Figs. 3–6 show that *hm*F2 makes a rapid drop in the ionosphere during most of the night-time conditions leading to an increase in the loss rate, L_0, of $O^+(^4S)$ ions in chemical reactions of these ions with unexcited and vibrationally excited N_2 and O_2 at *hm*F2. Thus, this night-time decrease in *hm*F2 leads to a strengthening of a drop in *Nm*F2, decreasing the value of $N_e^{-1}\frac{\partial}{\partial\Lambda}N_e$, and the resulting influence of the zonal $\boldsymbol{E}\times\boldsymbol{B}$ plasma drift on *Nm*F2 becomes stronger.

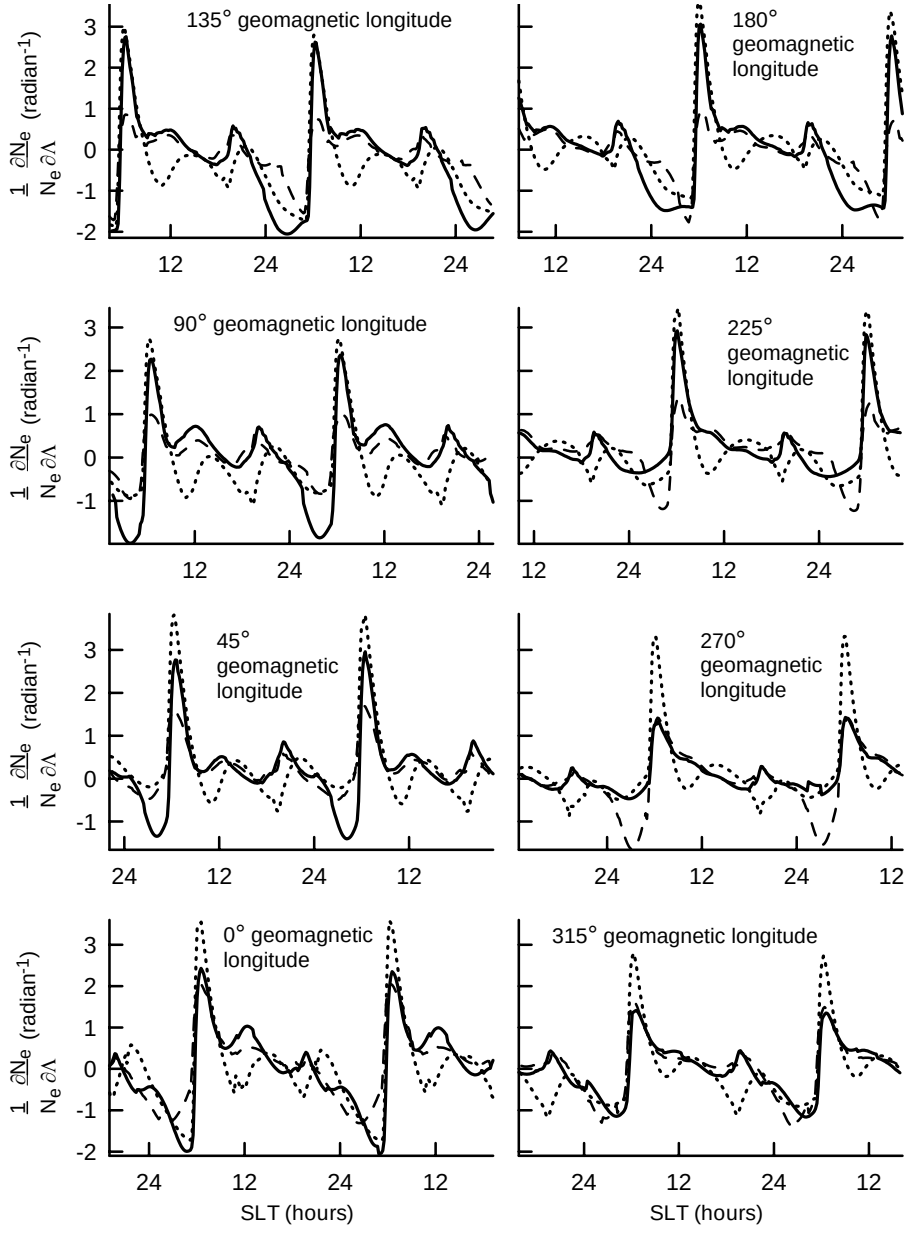

Fig. 10. The modeled value of $N_e^{-1}\frac{\partial}{\partial\Lambda}N_e$ at *hm*F2 as a function of SLT from 00:00 UT on 12 April 1958 to 24:00 UT on 13 April 1958 over the geomagnetic latitude of −15° (solid lines), 0° (dotted lines), and 15° (dashed lines) at the geomagnetic longitudes of 0°, 45°, 90°, 135°, 180°, 225°, 270°, and 315°.

The zonal $\boldsymbol{E}\times\boldsymbol{B}$ plasma drift, which is used in the model simulations, is directed from the geomagnetic west to the geomagnetic east by night, and the maximum eastward drift is about 165 m s^{-1} close to 20:45 SLT at F-region altitudes over the geomagnetic equator (see solid line in Fig. 2). After a peak before midnight, the magnitude of V_Λ^E at F-region altitudes over Jicamarca is observed to decrease with local time during the night-time period and during a part of the daytime period (after sunrise), reaching the minimum drift velocity at 11:15–12:15 SLT (see solid line in Fig. 2). Figure 8 shows the tendency of the influence of the zonal $\boldsymbol{E}\times\boldsymbol{B}$ plasma drift on *Nm*F2 to peak close to and after midnight, i.e. the *Nm*F2/*Nm*F2(V_Λ^E=0) ratio peaks a few hours later than V_Λ^E. It means that the night-time dependence of *Nm*F2 on V_Λ^E is essentially nonlocal in time, i.e. the value of *Nm*F2 at the fixed solar local time, t_1, depends on the values of V_Λ^E from t_0 to t_1, where t_0 is a solar local time at sunset. Furthermore, Fig. 10 shows that during most of the night-time period, the value of $N_e^{-1}\frac{\partial}{\partial\Lambda}N_e$ at *hm*F2 is decreased in time, strengthening the dependence of N_e on V_Λ^E. As a result, the influence of the eastward $\boldsymbol{E}\times\boldsymbol{B}$ plasma drift on *Nm*F2 is accumulated and, after a small drop, this effect is strengthened

in time up to a time point, with the following weakness of this influence. This conclusion can be illustrated from the reduced continuity equation for $O^+(^4S)$ ions, which takes into account only the loss rate of these ions and the zonal $\boldsymbol{E}\times\boldsymbol{B}$ plasma drift as (only for qualitative evaluations)

$$\frac{\partial}{\partial t}N_e = -L_0 N_e + V_\Lambda^E H^{-1} N_e, \quad (6)$$

where $H^{-1}=-(h_\Lambda N_e)^{-1}\frac{\partial}{\partial\Lambda}N_e$, t is SLT, and it was taken into account that $[O^+(^4S)]\approx N_e$ at altitudes of the F2-layer.

In virtue of Eq. (6), the night-time electron density decay is described as

$$N_e(t_1, q, U, \Lambda)=N_e(t_0, q, U, \Lambda)\exp\{-\int_{t0}^{t_1}(L_0-V_\Lambda^E H^{-1})dt\}. \quad (7)$$

It is evident from Eq. (7) that *Nm*F2(t_1) depends on the values of V_Λ^E and H from t_0 to t_1. The zonal $\boldsymbol{E}\times\boldsymbol{B}$ plasma drift cannot change N_e noticeably if changes in N_e in the $\boldsymbol{e}_\Lambda$ direction are feebly marked. On the other hand, changes in N_e due the zonal $\boldsymbol{E}\times\boldsymbol{B}$ plasma drift lead to a dependence of H on V_Λ^E. In addition to the daytime F2-region decay, during the night-time period, the meridional $\boldsymbol{E}\times\boldsymbol{B}$ drift moves ions and electrons from higher field lines to lower field lines, and, simultaneously, the plasma drifts due to neutral winds and diffuses along magnetic field lines, changing the magnitude of $N_e^{-1}\frac{\partial}{\partial\Lambda}N_e$ and the resulting effect of V_Λ^E on N_e.

As Fig. 2 shows, the night-time eastward drifts are considerably larger than the westward daytime drifts at F-region altitudes over the geomagnetic equator. Contrary to night-time conditions, the dependence of *Nm*F2 on V_Λ^E and $N_e^{-1}\frac{\partial}{\partial\Lambda}N_e$ cannot be illustrated by Eq. (7) and the effect of V_Λ^E on *Nm*F2 is not accumulated in time by day during a long time period. As a result, V_Λ^E produces small effects in *Nm*F2 during the studied daytime periods (see Figs. 3–6 and Fig. 8).

The night-time meridional $\boldsymbol{E}\times\boldsymbol{B}$ drift of electrons and ions moves the plasma from higher L-shells to lower L-shells and redistributes changes in electron and ion densities between field lines. Therefore, variations in N_i and N_e caused by the zonal $\boldsymbol{E}\times\boldsymbol{B}$ drift at magnetic field lines, which do not intersect the studied F-region altitudes, can lead to changes in the studied *hm*F2 and *Nm*F2. It follows from the model calculations that the night-time values of *hm*F2 and *Nm*F2 over the magnetic equator are weakly sensitive to variations in V_Λ^E at magnetic field lines, which cross the geomagnetic equator above about the 800–900 km height. The model simulations show that the $[NmF2/NmF2(V_\Lambda^E=0)]_{max}$ ratio over the geomagnetic equator at the 0–360° geomagnetic longitudes is less than 1.28 and 1.47, if $V_\Lambda^E=0$ at magnetic field lines, which cross the geomagnetic equator above 500 and 600 km height, respectively. It should be noted that $hmF2\leq 400$ km from 21:54–23:08 SLT to 24:00 SLT and from 00:00 SLT to 08:07–09:34 SLT over the geomagnetic equator, if the model employs the value of V_Λ^E described in Sect. 2. As a result, the zonal $\boldsymbol{E}\times\boldsymbol{B}$ plasma drift at magnetic field lines, which crosses the geomagnetic equator at F2-layer altitudes, cannot change *Nm*F2 very noticeably by night because during most of the night-time period, electron density changes in Λ at *hm*F2 at the same solar local time and geomagnetic longitude are less pronounced over the geomagnetic equator in comparison with those from about −10° to about −20° geomagnetic latitude or between about 10° and about 20° geomagnetic latitude (see Fig. 9). On the other hand, it follows from the model calculations presented by the solid line in the two lower panels of Fig. 6 that $[NmF2/NmF2(V_\Lambda^E=0)]_{max}\leq 2.27$ over the geomagnetic equator, if the value of V_Λ^E described in Sect. 2 is used. It means that the night-time dependence of *Nm*F2 on V_Λ^E is essentially nonlocal in space close to the geomagnetic equator.

Sterling et al. (1969) found no significant effects of V_Λ^E on *Nm*F2 without reporting the values of SLT and the geomagnetic longitudes and latitudes, where the Sterling et al. (1969) comparisons between separate calculations of N_e with and without the zonal $\boldsymbol{E}\times\boldsymbol{B}$ plasma drift were carried out. Contrary to the study by Sterling et al. (1969), it is found in this work that the effect of including the zonal $\boldsymbol{E}\times\boldsymbol{B}$ plasma drift in the model results in the maximum increase in the night-time *Nm*F2 up to a factor of 1.04–2.31 in the low latitude ionosphere between −20° and 20° geomagnetic latitude. It should be noted that there are significant differences between the meridional $\boldsymbol{E}\times\boldsymbol{B}$ plasma drift given by the empirical model of Scherliess and Fejer (1999) and that used by Sterling et al. (1969), and these differences can decrease the effect of V_Λ^E on N_e in the model simulations presented by Sterling et al. (1969). The zonal plasma drift measurements given by Fejer et al. (1981, 2005); Maynard et al. (1995); Sheehan and Valladares (2004) are in disagreement with the zonal component of $\boldsymbol{V}^E$ used by Sterling et al. (1969). For example, the zonal $\boldsymbol{E}\times\boldsymbol{B}$ plasma drift used by Sterling et al. (1969) is varied between $100\,m\,s^{-1}$ (close to 04:30 SLT) and $-100\,m\,s^{-1}$ (close to 16:30 SLT), while the average zonal F-region plasma drift measured over Jicamarca is varied from about $-50\,m\,s^{-1}$ (at 11:15–12:15 SLT) to about $165\,m\,s^{-1}$ (close to 20:45 SLT) during equinox at high solar activity (Fejer et al., 2005). It is possible to assume that the difference between V_Λ^E used by Sterling et al. (1969) and V_Λ^E described in Sect. 2 determines the difference or a part of the difference between the conclusion of this work and the conclusion given by Sterling et al. (1969).

Anderson (1981) has reinvestigated the effects of the zonal $\boldsymbol{E}\times\boldsymbol{B}$ plasma drift on the equatorial F-region ionosphere for March 1979 conditions, when the solar F10.7 cm flux was about 185 units, and has found that calculated F2-peak electron densities at the magnetic equator at 20:00 LT and at 24:00 LT do not differ significantly from *Nm*F2 obtained when the zonal $\boldsymbol{E}\times\boldsymbol{B}$ drift is omitted. Unfortunately, Anderson (1981) did not report the value of the geomagnetic longitude, which corresponds to these model results. On the other hand, the Jicamarca meridional and zonal $\boldsymbol{E}\times\boldsymbol{B}$ plasma drifts were used by Anderson (1981) in the model simulations, and,

it is reasonable to suppose that the model results presented in Fig. 10 of Anderson (1981) correspond to the Jicamarca Radio Observatory geomagnetic longitude of 357° for 1979.

It follows from the model simulations presented in panel (c) of Fig. 7 that the *Nm*F2/*Nm*F2(V_Λ^E=0) ratio is varied between 1.06 and 1.13 at 20:00 SLT on 12 April 1958 and from 0.99 to 1.26 at 24:00 SLT on 13 April 1958 over the geomagnetic equator. This ratio is close to 1.10 at 20:00 SLT and at 24:00 SLT on 11 April 1958 at 357° geomagnetic longitude over the geomagnetic equator. These model results and those presented by Anderson (1981) are purely comparable. It is also necessary to take into account that the observed zonal $\boldsymbol{E}\times\boldsymbol{B}$ plasma drift given by Fejer et al. (1981) at high solar activity at equinox was used by Anderson (1981) (see the dotted line in Fig. 2). This drift has a maximum amplitude of 120 $\mathrm{m\,s^{-1}}$ occurring at about 21:00 SLT, while the maximum value of the eastward zonal $\boldsymbol{E}\times\boldsymbol{B}$ plasma drift (Fejer et al., 2005) used in the model simulation of this work is equal to about 165 $\mathrm{m\,s^{-1}}$, close to 20:45 SLT, and the value of V_Λ^E given by Fejer et al. (2005) at high solar activity at equinox is larger than that given by Fejer et al. (1981) and used by Anderson (1981), from about 17:45 SLT to 24:00 SLT and from 00:00 SLT to about 03:00 SLT (compare the solid and dotted lines in Fig. 2). Therefore, a small excess of *Nm*F2/*Nm*F2(V_Λ^E=0) over that given by Anderson can be explained by the higher eastward zonal $\boldsymbol{E}\times\boldsymbol{B}$ plasma drift used in the model simulations of this work. There are also differences in the model inputs used in this work and those by Anderson (1981), e.g. the differences in the meridional $\boldsymbol{E}\times\boldsymbol{B}$ plasma drifts and in the neutral densities. These differences in the model inputs can lead to differences in the model results. Thus, the influence of the zonal $\boldsymbol{E}\times\boldsymbol{B}$ plasma drift on *Nm*F2 at 20:00 SLT and at 24:00 SLT on 12 April 1958 at 357° geomagnetic longitude over the geomagnetic equator found in this work does not conflict with the results of Fig. 10 presented by Anderson (1981).

6 Conclusions

A new three-dimensional, time-dependent theoretical model of the Earth's low and middle latitude ionosphere and plasmasphere has been developed on the basis of the two-dimensional time-dependent theoretical model of the Earth's low and middle latitude ionosphere and plasmasphere of Pavlov (2003), to take into account the effects of the zonal $\boldsymbol{E}\times\boldsymbol{B}$ plasma drift on N_i, N_e, T_e, and T_i. The new model uses a combination of the Eulerian and Lagrangian approaches. The electron and ion continuity, and energy equations are solved in a set of Lagrangian frames of reference. Each Lagrangian frame of reference moves with an individual plasma tube, with the local plasma drift velocity perpendicular to the magnetic and electric fields. As a result, only the time dependent, one-dimensional electron and ion continuity, and energy equations are solved in these Lagrangian frames of reference. The method makes use of an Eulerian computational grid, which is fixed in space coordinates and chooses the set of the plasma tubes at every time step, so that each plasma tube arrives at points which are located between two grid lines of the regularly spaced Eulerian computational grid at the next time step. The solution values of electron and ion densities and temperatures at the Eulerian computational grid are obtained by interpolation.

The new model calculates the number densities of $O^+(^4S)$, H^+, NO^+, O_2^+, N_2^+, $O^+(^2D)$, $O^+(^2P)$, $O^+(^4P)$, and $O^+(^2P^*)$ ions, N_e, T_e, and T_i using an eccentric tilted dipole approximation for the geomagnetic field. In the model, dipole orthogonal curvilinear coordinates q, U, and Λ are used, where q is aligned with, and U and Λ are perpendicular to, the magnetic field, and the U and Λ coordinates are constant along a dipole magnetic field line. The Eulerian computational grid used consists of a distribution of the dipole magnetic field lines in the ionosphere and plasmasphere at (q,U) planes, which are located at 72 geomagnetic longitudes Λ=0°, 5°,...355°. One hundred dipole magnetic field lines are used in the model for each fixed value of Λ. The number of the fixed nodes taken along each magnetic field line is 191. For each fixed value of the geomagnetic longitude, the Eulerian computational grid is located at a (q,U) plane, which is bounded by two dipole magnetic field lines. The low and upper boundary magnetic field lines intersect the geomagnetic equatorial point at 150 km altitude and 4264 km altitude, respectively. The Eulerian computational grid dipole magnetic field lines are distributed between these two boundary lines. The finite-difference algorithm yields approximations to N_i, N_e, T_i, and T_e in the ionosphere and plasmasphere, with the time step of 10 min. The interpolation procedure is used to find the values of N_i, N_e, T_i, and T_e at points which are located between 72 Eulerian computational grid (q,U) planes.

We have presented a comparison between the modeled *Nm*F2 and *hm*F2, and *Nm*F2 and *hm*F2, which were observed by the La Paz, Natal, Bombay, Ahmedabad, Trivandrum, Kodaikonal, Tiruchirapalli, Delhi, Calcutta, Singapore, Maui, Talara, Panama, Chiclayo, Huancayo, and Bogota ionospheric sounders during the geomagnetically quiet time period of 12–13 April 1958 at high solar activity. The model reproduces major features of the data if the equatorial meridional $\boldsymbol{E}\times\boldsymbol{B}$ plasma drift and the NRLMSISE-00 [O] are corrected. The comparison between the modeled *Nm*F2 and *Nm*F2 measured by the ionosondes show that it is necessary to decrease the NRLMSISE-00 model [O] ratio by a factor, which is varied between 1.2 and 1.5, depending on the geomagnetic latitude and longitude. To bring the measured and modeled *Nm*F2 and *hm*F2 into better agreement, the model meridional $\boldsymbol{E}x\boldsymbol{B}$ plasma drift was changed from the Scherliess and Fejer (1999) model value to 20 $\mathrm{m\,s^{-1}}$ between 16:00 SLT and 20:00 SLT at each geomagnetic longitude over the geomagnetic equator, if this drift exceeded 20 $\mathrm{m\,s^{-1}}$.

In agreement with the generally accepted assumption based on the work of Anderson (1981), the changes in *Nm*F2

due to the zonal $\boldsymbol{E}\times\boldsymbol{B}$ plasma drift are found to be inessential by day, and the influence of the zonal $\boldsymbol{E}\times\boldsymbol{B}$ plasma drift on *Nm*F2 and *hm*F2 is found to be negligible above about 25° and below about −26° geomagnetic latitude by day and by night. Contrary to common belief, it is shown that the zonal $\boldsymbol{E}\times\boldsymbol{B}$ plasma drift forms a plasma source for the night-time ionosphere and the effect of including the zonal $\boldsymbol{E}\times\boldsymbol{B}$ plasma drift in the model results in the maximum increase of night-time *Nm*F2 up to a factor of 1.04–2.31 in the low-latitude ionosphere between −20° and 20° geomagnetic latitude. This night-time increase in *Nm*F2 is less pronounced at −20° and 20° geomagnetic latitudes in comparison with that between −10° and 10° geomagnetic latitude. An examination of the influence of the zonal $\boldsymbol{E}\times\boldsymbol{B}$ plasma drift on *Nm*F2 shows marked variations in geomagnetic longitude. In the night-time low-latitude ionosphere between −10° and 10° geomagnetic latitude, the enhancements in *Nm*F2 due to the zonal $\boldsymbol{E}\times\boldsymbol{B}$ plasma drift are more pronounced close to 140° geomagnetic longitude, and the model also produces the second peak in $[NmF2/NmF2(V_{\Lambda}^{E}=0)]_{\max}$ from 330° to 345° geomagnetic longitude. The influence of the zonal $\boldsymbol{E}\times\boldsymbol{B}$ plasma drift on the night-time F2-peak density is less pronounced close to 20–35° geomagnetic longitude and near 245–275° geomagnetic longitude between −10° and 10° geomagnetic latitude. It is shown that the longitude variations found in the influence of the zonal $\boldsymbol{E}\times\boldsymbol{B}$ plasma drift on *Nm*F2 are mainly caused by the longitudinal asymmetry in $\boldsymbol{B}$ (the eccentric magnetic dipole is displaced from the Earth's center and the Earth's eccentric tilted magnetic dipole moment is inclined with respect to the Earth's rotational axis), by the variations in the wind induced plasma drift in geomagnetic longitude, and by the variations of the meridional $\boldsymbol{E}\times\boldsymbol{B}$ plasma drift in geomagnetic longitude (due to the longitudinal dependence of the meridional equatorial $\boldsymbol{E}\times\boldsymbol{B}$ plasma drift produced by the empirical model of Scherliess and Fejer, 1999).

Acknowledgements. Hourly critical frequencies *fo*F2, *fo*E and maximum usable frequency parameters *M*(3000)F2 data from the ionospheric sounder stations were provided by the National Geophysical Data Center, Boulder, Colorado. A. V. Pavlov was supported by grant 06-05-64179 from the Russian Foundation for Basic Research. The author of the paper acknowledges B. G. Fejer and L. Schlerliess for providing me by the Fortran code of the empirical model of the plasma drift over the geomagnetic equator for quiet conditions. The author would like to thank referees for their comments on the paper, which have assisted in improving the final version.

Topical Editor M. Pinnock thanks M. Denton and Y. Sahai for their help in evaluating this paper.

References

Abdu, M. A.: Major phenomena of the equatorial ionosphere-thermosphere system under disturbed conditions, J. Atmos. Terr. Phys., 59, 1505–1519, 1997.

Abdu, M. A.: Outstanding problems in the equatorial ionosphere-thermosphere electrodynamics relevant to spread F, J. Atmos. Sol. Terr. Phys., 63, 869–884, 2001.

Anderson, D. N.: A theoretical study of the ionospheric F region equatorial anomaly – I. Theory, Planet. Space Sci., 21, 409–419, 1973a.

Anderson, D. N.: A theoretical study of the ionospheric F region equatorial anomaly – II. Results in the American and Asian sectors, Planet. Space Sci., 21, 421–442, 1973b.

Anderson, D. N.: Modeling the ambient, low latitude F-region ionosphere – A review, J. Atmos. Terr. Phys., 43, 753–762, 1981.

Anderson, D. N., Decker, D. T., and Valladares, C. E.: Global theoretical ionospheric model (GTIM), in: Handbook of Ionospheric Models, edited by: Schunk, R. W., pp. 133–152, Utah State Univ., Logan, Utah, 1996.

Bailey, G. J. and Balan, N.: A low-latitude ionosphere-plasmasphere model, in: Handbook of Ionospheric Models, edited by: Schunk, R. W., pp. 173–206, Utah State Univ., Logan, Utah, 1996.

Deminov, M. G. and Fishchuk, Y. A.: On the use of the geomagnetic field approximation by the eccentric dipole in problems of ionosphere and plasmasphere, Geomagnetism and Aeronomy, 40, 383–387, 2000.

Dudeney, J. R.: The accuracy of simple methods for determining the height of the maximum electron concentration of the F2-layer from scaled ionospheric characteristics, J. Atmos. Terr. Phys., 45, 629–640, 1983.

Fejer, B. G.: F region plasma drifts over Arecibo – Solar cycle, seasonal, and magnetic activity effects, J. Geophys. Res., 98, 13 645–13 652, 1993.

Fejer, B. G., Farley, D. G., and Gonzalez, S. A.: F region east-west drifts at Jicamarca, J. Geophys. Res., 86, 215–218, 1981.

Fejer, B. G. and Scherliess, L.: On the variability of equatorial F-region vertical plasma drifts, J. Atmos. Sol. Terr. Phys., 63, 893–897, 2001.

Fejer, B. G., Souza, J. R., Santos, A. S., Costa Pereira, A. E.: Climatology of F region zonal plasma drifts over Jicamarca, J. Geophys. Res., 110, 12 310, doi:10.1029/2005JA011324, 2005.

Fesen, C. G., Hysell, D. L., Meriwether, J. M., Mendillo, M., Fejer, B. G., Roble, R. G., Reinisch, B. W., and Biondi, M. A.: Modeling the low-latitude thermosphere and ionosphere, J. Atmos. Sol. Terr. Phys., 64, 1337–1349, 2002.

Fraser-Smith, A. C.: Centered and eccentric geomagnetic dipoles and their poles, 1600–1985, Rev. Geophys., 25, 1–16, 1987.

Hedin, A. E.: MSIS-86 thermospheric model, J. Geophys. Res., 92, 4649–4662, 1987.

Hedin, A. E., Spencer, N. W., Biondi, M. A., Burnside, R. G., Hernandez, G., and Johnson, R. M.: Revised global model of thermosphere winds using satellite and ground-based observations, J. Geophys. Res., 96, 7657–7681, 1991.

Huba, J. D., Joyce, G., and Fedder, J. A.: Sami2 is another model of the ionosphere (SAMI2): A new low-latitude ionosphere model, J. Geophys. Res., 105, 23 035–23 054, 2000.

Lean, J. L., Picone, J. M., Emmert, J. T., and Moore, G.: Thermospheric densities derived from spacecraft orbits: applica-

tion to the Starshine satellites, J. Geophys. Res., 110, 4301, doi:10.1029/2005JA011399, 2006.

Maruyama, N., Watanabe, S., and Fuller-Rowell, T. J.: Dynamic and energetic coupling in the equatorial ionosphere and thermosphere, J. Geophys. Res., 108, 1396, doi:10.1029/2002JA009599, 2003.

Maynard, N. L., Aggson, T. L., Herrero, F. A., Liebrecht, M. C., and Saba, J. L.: Average equatorial zonal and vertical ion drifts determined from San Marco D electric field measurements, J. Geophys. Res., 100, 17 467–17 479, 1995.

Millward, G. H., Moffett, R. J., Quegan, S., and Fuller-Rowell, T. J.: A coupled thermosphere-ionosphere-plasmasphere model (CTIP), in: Handbook of Ionospheric Models, edited by: Schunk, R. W., pp. 239–279, Utah State Univ., Logan, Utah, 1996.

Moffett, R. J.: The Equatorial Anomaly in the Electron Distribution of the Terrestrial F-Region, Fundamentals of Cosmic Physics, 4, 313–391, 1979.

Pavlov, A. V.: The role of vibrationally excited oxygen and nitrogen in the ionosphere during the undisturbed and geomagnetic storm period of 6–12 April 1990, Ann. Geophys., 16, 589–601, 1998, http://www.ann-geophys.net/16/589/1998/.

Pavlov, A. V.: New method in computer simulations of electron and ion densities and temperatures in the plasmasphere and low-latitude ionosphere, Ann. Geophys., 21, 1601–1628, 2003, http://www.ann-geophys.net/21/1601/2003/.

Pavlov, A. V., Fukao, S., and Kawamura, S.: Comparison of the measured and modeled electron densities and electron and ion temperatures in the low latitude ionosphere during 19–21 March 1988, Ann. Geophys., 22, 2747–2763, 2004a.

Pavlov, A. V., Fukao, S., and Kawamura, S.: F region ionospheric perturbations in the low-latitude ionosphere during the geomagnetic storm of 25–27 August 1987, Ann. Geophys., 22, 3479–3501, 2004b.

Pavlov, A. V. and Pavlova, N. M.: Causes of the mid-latitude *Nm*F2 winter anomaly at solar maximum, J. Atmos. Sol. Terr. Phys., 67, 862–877, 2005.

Pavlov, A.V., Fukao, S., and Kawamura, S.: A modeling study of ionospheric F2-region storm effects at low geomagnetic latitudes during 17–22 March 1990, Ann. Geophys., 24, 915–940, 2006, http://www.ann-geophys.net/24/915/2006/.

Picone, J. M., Hedin, A. E., Drob, D. P., and Aikin, A. C.: NRLMSISE-00 empirical model of the atmosphere: statistical comparisons and scientific issues, J. Geophys. Res., 107(A12), 1468, doi:10.1029/2002JA009430, 2002.

Richards, P. G., Fennelly, J. A., and Torr, D. G.: EUVAC: A solar EUV flux model for aeronomical calculations, J. Geophys. Res., 99, 8981–8992, 1994, Correction in: J. Geophys. Res., 99, 13 283, 1994.

Richards, P. G. and Torr, D. G.: The field line interhemispheric plasma model, in: Handbook of Ionospheric Models, edited by: Schunk, R. W., pp. 207–216, Utah State Univ., Logan, Utah, 1996.

Richmond, A. D. and Lu, G.: Upper-atmospheric effects of magnetic storms: a brief tutorial, J. Atmos. Terr. Phys., 62, 1115–1127, 2000.

Rishbeth, H.: The equatorial F-layer: progress and puzzles, Ann. Geophys., 18, 730–739, 2000, http://www.ann-geophys.net/18/730/2000/.

Rishbeth, H. and Müller-Wodarg, I. C. F.: Vertical circulation and thermospheric composition: a modelling study, Ann. Geophys., 17, 794–805, 1999, http://www.ann-geophys.net/17/794/1999/.

Roble, R. G.: The NCAR thermosphere-ionosphere-mesosphere-electrodynamics general circulation model (TIME-GCM), in: Handbook of Ionospheric Models, edited by: Schunk, R. W., pp. 281–288, Utah State Univ., Logan, Utah, 1996.

Schunk, R. W. and Sojka, J. J.: USU model of the global ionosphere, in: Handbook of Ionospheric Models, edited by: Schunk, R. W., pp. 281–288, Utah State Univ., Logan, Utah, 1996.

Scherliess, L. and Fejer, B. G.: Radar and satellite global equatorial F region vertical drift model, J. Geophys. Res., 104, 6829–6842, 1999.

Sheehan, R. and Valladares, C.: Equatorial ionospheric zonal drift model and vertical drift statistics from UHF scintillation measurements in South America, Ann. Geophys., 22, 3177–3193, 2004, http://www.ann-geophys.net/22/3177/2004/.

Shimazaki, T.: World-wide variations in the height of the maximum electron density of the ionospheric F2 layer, J. Radio Res. Labs. Japan, 2(7), 85–97, 1955.

Sterling, D. L., Hanson, W. B., Moffett, R. J., and Baxter, R. G.: Influence of electromagnetic drifts and neutral air winds on some features of the F_2 region, Radio Sci., 4, 1005–1023, 1969.

Souza, J. R., Abdu, M. A., Batista, I. S., and Bailey, G. J.: Determination of vertical plasma drift and meridional wind using the Sheffield University Plasmasphere Ionosphere Model and ionospheric data at equatorial and low latitudes in Brazil: Summer solar minimum and maximum conditions, J. Geophys. Res., 105, 12 813–12 821, 2000.

Walker, G. O.: Longitudinal structure of the F-region equatorial anomaly – A review, J. Atmos. Terr. Phys., 43, 763–774, 1981.